

The Wreaths of KHAN: Uniform Graph Feature Selection with False Discovery Rate Control

Jiajun Liang^{1,*} Yue Liu^{2,*} Doudou Zhou³ Sinian Zhang⁴ Junwei Lu^{3,†}

Abstract

Graphical models find numerous applications in biology, chemistry, sociology, neuroscience, etc. While substantial progress has been made in graph estimation, it remains largely unexplored how to select significant graph signals with uncertainty assessment, especially those graph features related to topological structures including cycles (i.e., wreaths), cliques, hubs, etc. These features play a vital role in protein substructure analysis, drug molecular design, and brain network connectivity analysis. To fill the gap, we propose a novel inferential framework for general high dimensional graphical models to select graph features with false discovery rate controlled. Our method is based on the maximum of p -values from single edges that comprise the topological feature of interest, thus is able to detect weak signals. Moreover, we introduce the K -dimensional persistent Homology Adaptive selection (KHAN) algorithm to select all the homological features within K dimensions with the uniform control of the false discovery rate over continuous filtration levels. The KHAN method applies a novel discrete Gram-Schmidt algorithm to select statistically significant generators from the homology group. We apply the structural screening method to identify the important residues of the SARS-CoV-2 spike protein during the binding process to the ACE2 receptors. We score the residues for all domains in the spike protein by the p -value weighted filtration level in the network persistent homology for the closed, partially open, and open states and identify the residues crucial for protein conformational changes and thus being potential targets for inhibition.

Keyword: Graphical models, combinatorial inference, multiple testing, false discovery control.

1 Introduction

Graphical models are a prevalent tool for modeling relationships between variables. They are widely used in various fields, especially certain sub-structures of the graphs between variables is of great interest. In biology, proteins are vital to life and their practical function is highly influenced by their unique sub-structure, which is determined by the combination of amino acids. For example, the Y-shape of an antibody enables it to bind to antigens like bacteria and viruses with one end and to other immune-system proteins with the other end (Janeway Jr et al., 2001). Similarly, the

¹Department of Statistics, Purdue University, West Lafayette, IN 47906

²Department of Statistics, Harvard University, Cambridge, MA 02138

³Department of Biostatistics, Harvard Chan School of Public Health, Boston, MA 02130

⁴School of Statistics, Renmin University of China, Beijing, China 100872

* Equal contribution

† Corresponding author (junweilu@hsph.harvard.edu)

“wreath” shape of the DNA polymerase III holoenzyme facilitates the efficient formation of a ring around DNA, enabling fast DNA synthesis (Kelman and O’Donnell, 1995; Clark and Pazdernik, 2013). Alphabet/Google is developing AlphaFold to predict the structures of proteins with a reinforcement learning approach (Jumper et al., 2021; Evans et al., 2021). In chemistry, a critical task is modeling molecular structures, which determine their pharmacological and ADME/T properties (absorption, distribution, metabolism, excretion, and toxicity). For instance, the presence of the cyanide group makes hydrogen cyanide (HCN) highly toxic, leading to potential death within minutes (Council et al., 2002). High-Density Polyethylene (HDPE) has a linear structure, offering density and strength for products requiring rigidity, such as milk jugs and water pipes. Conversely, Low-Density Polyethylene (LDPE), with its branched structure, is suited for flexible applications, including plastic bags and squeeze bottles (Fried, 2014). In neuroscience, cliques within the brain network are vital as they are neurologically strongly associated with efficient support of behavior (Bassett and Sporns, 2017; Wang et al., 2021). In sociology, social networks play an important role in understanding behavior among individuals or organizations and making social recommendations or marketing strategies. For instance, the presence of a “hub” structure in the social network indicates that the central user is active and influential, as they are connected to many other users. Therefore, the advertising industry often targets these individuals with free samples to increase their reputation, rather than selecting people at random (Ilyas et al., 2011; Li et al., 2018; Lee et al., 2019). In this paper, we mainly focus on the application of the SARS-CoV-2 spike protein sub-structure analysis. To identify the potential targets for inhibition in the vaccine design, we aim to select the protein sub-structures persistently vary in the binding process to the ACE2 receptors (Ou et al., 2020).

Despite the vast applications of the sub-structure detection of graphical models mentioned above, the majority of existing research focused on the edge-wise inference (Cai et al., 2011; Fan et al., 2016; Cai et al., 2016; Ding and Zhou, 2020). The majority literature of the statistical methods on the false discovery control (Benjamini, 2010; Van de Geer et al., 2014; Li and Maathuis, 2021) worked on selecting the parametric signals which cannot be directly applied to the discrete graph sub-structures selection. This paper aims to bridge the gap by proposing the selecting the graph topological features with the false discovery rate control. We also propose to screen topological features persistent under continuous filtration levels utilizing the framework of the persistent homology (Horak et al., 2009; Aktas et al., 2019). In specific, let $G^* = (V, E^*)$ represents the true undirected graph, where $V = \{1, 2, \dots, d\}$ is the collection of nodes and E^* is the edge set of the graph. Suppose $\mathcal{F} = \{F_1, F_2, \dots, F_J\}$ is the set consisting of all graph features of interest in G^* that we aim to select, where J is the cardinality of candidate graph features. Examples of such graph features include cliques, which are fully connected subsets of nodes, and loops, which are closed paths within the graph. We consider the multiple hypotheses testing whether each graph feature $F_j \in \mathcal{F}$ can be embedded into the true graph G^* , i.e.,

$$H_{0j} : F_j \not\subseteq G^* \quad \text{v.s.} \quad H_{1j} : F_j \subseteq G^*, \quad 1 \leq j \leq J, \quad (1.1)$$

where $F \subseteq G^*$ means F is a subgraph of G^* . In order to test these hypotheses with false discovery rate controlled, we consider the maximum p -value among all edges within F_j . This approach differs significantly from previous methods in combinatorial inference (Shen and Lu, 2023; Liu et al., 2023; Zhang and Lu, 2024), which adjust the multiplicity by the maximum statistic and maximal Gaussian multiplier bootstrap. In comparison, our proposed method only requires single edge p -values and therefore can detect weaker signals and is also computationally more efficient.

Besides selecting the given graph features, we also consider to evaluate the strength of these signals at multiple scales. The network persistent homology (Horak et al., 2009; Lee et al., 2012; Aktas et al., 2019) and the persistent barcode (Ghrist, 2008; Kovacev-Nikolic et al., 2016) are powerful tools for analyzing and measuring the persistence of multiple homological features, such as triangles, tetrahedrons, and higher-dimensional polytopes. However, few methods have been developed to quantify the uncertainty when inferring the network persistent homology from noisy datasets. We solve this problem by considering the multiple hypotheses at the filtration level μ as

$$\begin{aligned} H_{0j}(\mu) &: \text{the } j\text{-th homological feature } \not\subseteq G^*(\mu), \\ \text{v.s. } H_{1j}(\mu) &: \text{the } j\text{-th homological feature } \subseteq G^*(\mu), \end{aligned} \tag{1.2}$$

where $G^*(\mu)$ is the filtered graph at level μ and the homological feature is a group generator of the graph homology group which we will define in details in Section 2. Intuitively, a K -dimensional homological feature is a K -dimensional “wreaths” on the graph as a discrete analogue of a K -dimensional sphere in Euclidean space. Figure 1 illustrates the 1-dimensional and 2-dimensional homological features and how they appear with the change of the filtration level.

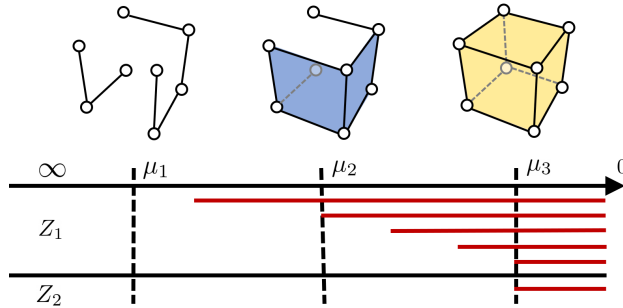


Figure 1: Illustration of the filtered graph, homological features, and the persistent barcode. Two 1-dimensional homological features (blue, i.e., $\text{rank}(Z_1(E(\mu_2))) = 2$) show up at μ_2 and a 2-dimensional homological feature (yellow, i.e., $\text{rank}(Z_2(E(\mu_3))) = 1$) appears at μ_3 .

Our goal is to screen all the homological features under the given dimension K , with detailed definition in Section 2.1. We could not directly apply the approach for testing graph features in (1.1), as the candidate group generators could be linearly dependent. To tackle the double dependency: the probabilistic dependency among testing statistics and linear dependency among the generators in the homology group, we propose a novel discrete Gram-Schmidt p -value screening method to select the linearly independent homological features at any given filtration level. The algorithm is a homological analogue of the Gram-Schmidt algorithm which iteratively selects the generator with the smallest p -value among the subgroup which is linearly independent of the currently selected generators. The other challenge is to guarantee the false discovery rate of the selected homological features is uniformly controlled over continuous filtration levels. Instead of conducting the screening for each filtration level μ , our method adaptively identifies the change points in the persistent barcode in Figure 1 which is both computationally and statistically efficient. This results in the K -dimensional persistent Homology Adaptive selectioN (KHAN) algorithm. See Section 3.2 for the details. We introduce the new concept of uniform False Discovery Rate (uFDR) to quantify the performance of persistent homology over the continuous filtration levels and prove that our algorithm can handle the double dependency and control uFDR at the given level.

1.1 Related Work

Learning graph structures has been widely studied in the existing literature. There have been many significant progress on recovering the underlying graph by estimation. For the Gaussian graphical model, many works estimate the graph through estimating the inverse covariance matrix Θ^* where $\Theta_{uv}^* \neq 0$ if and only if the edge $(u, v) \in E^*$ (Meinshausen and Bühlmann, 2006; Friedman et al., 2008; Lam and Fan, 2009; Peng et al., 2009; Ravikumar et al., 2011; Cai et al., 2011; Shen et al., 2012). For the Ising model, which consists of discrete variables (+1 or -1), the estimation of parameters is achieved by using penalized logistic regression (Ravikumar et al., 2010), and the study of parameter estimation and inference is furthered through the maximum pseudo-likelihood estimate (Bhattacharya and Mukherjee, 2018).

Persistent homology is a powerful tool to analyze topological features over these graphs, which involves tracking the birth and death of topological features along filtrations of graphs (Horak et al., 2009; Aktas et al., 2019). However, the primary focus of these studies has been on extracting the persistent topological features of a deterministic networks without the uncertainty quantification of the graph estimation error. An inferential method is proposed (Fasy et al., 2014) to construct confidence set for the persistence diagrams for the landscape of probability density functions. However, this method is restricted to the persistent homology of Euclidean spaces, and cannot be applied to discrete networks.

For the inferential methods on graphical models, most literature has focused on continuous quantities and local properties of graph (e.g., presence of edges) (Cai and Ma, 2013; Jankova and Van De Geer, 2015; Ren et al., 2015; Cai and Zhang, 2016; Chen et al., 2016; Neykov et al., 2018). For instance, hypothesis tests for the covariance matrix have been constructed (Cai and Ma, 2013), tests for the presence of edges in the Gaussian graphical model have been developed (Ren et al., 2015), and considerations for the estimation and testing of high-dimensional differential correlation matrices have been proposed (Cai and Zhang, 2016). Regarding multiple tests in graphical models, efforts have been made to select edges with false discovery rate (FDR) control using the Benjamini-Hochberg method (Benjamini and Hochberg, 1995), and methodologies have been developed to learn the structure of Gaussian graphical models with FDR control based on the knockoff framework (Li and Maathuis, 2021). However, a critical gap in this corpus of work is its focus on methodologies primarily for continuous parameters, and it is challenging to apply those techniques to select discrete graph features addressed in this paper.

Research on the combinatorial structure and global properties of graphs has led to proposals for testing monotone properties within the Gaussian graphical model, such as connectivity, the maximum degree, and cycle presence (Lu et al., 2017). Similar efforts have been directed towards testing graph properties in the Ising model (Neykov and Liu, 2019; Jin et al., 2020). However, these methodologies are limited as they are designed for conducting single tests without controlling the FDR. Addressing the challenge of simultaneous multiple testing, the StarTrek algorithm for selecting hub nodes based on a pre-specified degree threshold in graphs has been proposed (Zhang and Lu, 2024). However, the StarTrek procedure (Zhang and Lu, 2024) is primarily designed for selecting hub nodes, whereas our goal is to select general graph features of interest including the hub nodes. In comparison, is much more complicated and challenging, with broader applications. In methodology, the StarTrek procedure involves the use of the maximal statistic for uniform control over edges and the Gaussian multiplier bootstrap for quantile estimation, which are statistically conservative and computationally intensive. In contrast, our proposed method does not require the use of either the maximal statistic or the Gaussian multiplier bootstrap, making it simpler and more

efficient. Moreover, our method can be applied to study the persistence of graph features within the framework of persistent homology and offers stronger false discovery control across multiple scales.

1.2 Our Contributions

In methodology, we propose a novel inferential framework to select general graph structural features with false discovery rate control. One of the challenge problem is to assign each structural feature with a p -value. Compared to the estimation of the p -values of edges, the estimation of the p -value of a graph structure requires combinatorial and uniform control on involved edges for multiple cases. As a result, the estimation of the p -values of edges within and between structures could be highly dependent. To address this issue, maximal statistics have been used in the literature (Zhang and Lu, 2024). However, computing p -values for maximal statistics can be computationally intensive and statistically conservative. In comparison, our method is based on the maximum of single-edge p -values which becomes faster in computation and more efficient in detecting weaker signals. Based on that, this paper also introduces a novel KHAN algorithm which can adaptively select homological features from the network persistent barcode over continuous filtration level. The KHAN algorithm is based on a discrete Gram-Schmidt p -value screening method which untangles the probabilistic and algebraic dependency among the candidate generators in the homology group. The method also provides adaptive selection procedure for the change points on the filtration of the persistent barcode, and thus is computationally efficient. To the best of our knowledge, it is the first time for our paper to propose inferential method for selecting homological features from the network persistent homology with FDR controlled.

In theory, the proposed KHAN framework is guaranteed to achieve FDR control and be powerful under reasonable sparsity and dependence conditions for general structural features and general graphical models. We introduce the uniform false discovery rate (uFDR) on continuous scales and show the proposed method can have the uFDR controlled at the given level only using the single-edge p -values, and developing uniform false discovery control. Compared to the Cramér-type inequality for the maximal statistics in Gaussian graphical model in Zhang and Lu (2024), we propose novel theoretic analysis for FDR for t -statistics and covers the general family of graphical models. Our proof technique can handle the dependency among p -values of structural features and control the FDR as long as their correlations are not too strong. This analysis approach can be applied to the proof of uFDR control even the dependency among infinite filtration levels are involved.

In application, we implement the proposed method to select residues of interest in the SARS-CoV-2 Spike protein during the binding process. Compared the existing works (Ou et al., 2020; Ray et al., 2021; Liu et al., 2020) using marginal correlations to identify the vital residues involving the receptor-binding domain, our analysis applies the graphical model incorporating the conditional dependency and the network persistent homology considering the structural changes. Therefore, we are able to take into account all four domains: NTB, RBD, linker, and S2 in the protein and their interactions during the conformational changes.

1.3 Notations

We denote set $A \times B = \{(a, b) : a \in A, b \in B\}$. Let G^* be a true graph with vertex set V and edge set E^* , and let G be an arbitrary graph that may differ in different instances. We

define $\bar{E} = \{(x, y) : x, y \in V, x \neq y\}$ to be the complete edge set. We define $E(\cdot)$ to be a function where $E(G)$ gives the edge set of graph G , and we define $V(G)$ be the vertex set of graph G . We say $G \subseteq G'$ if and only if $V(G) \subseteq V(G')$ and $E(G) \subseteq E(G')$. $\Phi(\cdot)$ is the cumulative distribution function of the standard Gaussian. For a sequence of random variables $\{X_n\}_{n=1}^\infty$ and a scalar a , we say $X_n \leq a + o_P(1)$ if and only if $\lim_{n \rightarrow \infty} \mathbb{P}(X_n - a > \epsilon) = 0$ for all $\epsilon > 0$. We say $f = O(g)$ if $f \leq Cg$ for some constant C , and $f = o(g)$ and $g = \omega(f)$ if $C \rightarrow 0$. Define the set $[n] = \{1, 2, \dots, n\}$. We use $|A|$ to denote the cardinality of a set A . For a vector $v = (v_1, \dots, v_d)^T \in \mathbb{R}^d$, and $1 \leq q \leq \infty$, we define norm of v as $\|v\|_q = \left(\sum_{i=1}^d |v_i|^q\right)^{1/q}$. In particular, $\|v\|_0 = \sum_{1 \leq i \leq d} \mathbb{I}\{v_i \neq 0\}$. For a matrix $\mathbf{M} \in \mathbb{R}^{r \times c}$, we use $\mathbf{M}_{\cdot j}$ and \mathbf{M}_j to denote the j -th column and row of \mathbf{M} correspondingly. Additionally, let $\|\mathbf{M}\|_p = \max_{\|v\|_p=1} \|\mathbf{M}v\|_p$ for $p \geq 1$. In particular, $\|\mathbf{M}\|_1 = \max_{1 \leq j \leq c} \sum_{i=1}^r |\mathbf{M}_{ij}|$. If \mathbf{M} is symmetric, let $\lambda_{\max}(\mathbf{M})$ and $\lambda_{\min}(\mathbf{M})$ denote the largest and smallest eigenvalues correspondingly. We denote $\Phi(\cdot)$ as the standard normal cumulative density function.

2 Graph Feature Selection

In this section, we first provide some preliminaries on the concept of the graphical model and the graph feature selection problem. Then, we introduce the method for the sub-problem of selecting general graph features.

2.1 Graphical Model and Persistent Homology

In our paper, we consider the general graphical model. Let $\mathbf{X} = (X_1, \dots, X_d)^T \in \mathbb{R}^d$ be a random vector indexed by the nodes of the true graph $G^* = (V, E^*)$, i.e., the node j of the graph corresponds to the random variable X_j . The graph is assigned with the edge weights matrix $W^* = \{W_e^*\}_{e \in \bar{E}} \in \mathbb{R}^{d \times d}$ and the graphical model implies the conditional dependency that X_j is independent to X_k conditioning on all other variables if and only if $(j, k) \notin E^*$. The connection between the edges and the weights can typically be distilled into two distinct scenarios, both of which are covered in this paper:

$$\begin{aligned} \text{Scenario (a): } E^* &= \{e \in \bar{E} : |W_e^*| > 0\}, \\ \text{Scenario (b): } E^* &= \{e \in \bar{E} : W_e^* > 0\}. \end{aligned} \tag{2.1}$$

Scenario (a) delineates a two-sided case, where both negative and positive values of W^* are considered as edges. Conversely, Scenario (b) is indicative of a one-sided case, where only positive values of W^* are considered edges. For example, the Gaussian graphical model belongs to the Scenario (a). In specific, \mathbf{X} follows a multivariate Gaussian distribution $N_d(\mathbf{0}, \Sigma^*)$ with mean vector $\mathbf{0}$ and covariance matrix Σ^* . The weights are the entries of the precision matrix $W^* = (\Sigma^*)^{-1}$ and $e \in E^*$ if and only if $W_e^* \neq 0$. On the other hand, the ferromagnetic Ising model belongs to the Scenario (b) with the edge weights $W_{uv}^* = \mathbb{E}[X_u X_v] - \tanh(\theta)$ and $e \in E^*$ whenever $W_e^* > 0$. We will discuss the details of these two models in Examples 2.1 and 2.2.

Similar to (2.1), we define the graph at filtration level μ as $G^*(\mu) = (V, E^*(\mu))$ under two scenarios:

$$\begin{aligned} \text{Scenario (a): } E^*(\mu) &= \{e \in E^* : |W_e^*| > \mu\}, \\ \text{Scenario (b): } E^*(\mu) &= \{e \in E^* : W_e^* > \mu\}. \end{aligned}$$

Therefore, for a sequence of levels $\mu^{(1)} < \mu^{(2)} < \dots < \mu^{(t)}$, we can obtain a filtration of edge sets $E^*(\mu^{(1)}) \supseteq E^*(\mu^{(2)}) \supseteq \dots \supseteq E^*(\mu^{(t)})$ and a corresponding filtration of graphs

$$G^*(\mu^{(1)}) \supseteq G^*(\mu^{(2)}) \supseteq \dots \supseteq G^*(\mu^{(t)}). \quad (2.2)$$

We now define the network homology group. Given a graph $G = (V, E)$, we consider the k -th order chain group $C_k(E)$ consisting of k -cliques and the cycle group $Z_k(E)$ is the kernel of the the boundary operator ∂_k . A persistent barcode is a graphical representation where horizontal line segments encode the birth-death filtration ranges of generators across a given interval $[\mu_0, \mu_1]$, with the vertical axis represents the dimension k . We illustrate the graph filtration and the barcode in Figure 1 and refer the detailed definition of these concepts to Section A in the Supplementary Material. In this paper, we consider the cycle group as the homology group without taking the quotient in order to involve cliques as the features of interest as well. In the following of the paper, we will refer the homology group to the cycle group and vice versa. The persistent homology groups are the sequence of groups $Z_k(E(\mu))$ for multiple filtration levels. In this paper, we focus on selecting the generators of $Z_k(E(\mu))$, i.e., the homological features or the segments in the barcode, for all dimensions $k \leq K$. We formulate the multiple hypotheses in (1.2) by the homological notations. Denote the homology group given edge set E and the maximum dimension K as $Z(E) = \bigoplus_{1 \leq k \leq K} Z_k(E)$, where $K \leq d$ is the maximum homology dimension of interest and define $Z(\mu) = Z(\widehat{E}^*(\mu))$. In order to quantify the selection uncertainty, we introduce the uniform False Discovery Proportion (uFDP) over a filtration interval $[\mu_0, \mu_1]$:

$$\text{uFDP} = \sup_{\mu \in [\mu_0, \mu_1]} \frac{\text{rank}(\widehat{Z}(\mu)) - \text{rank}(Z(\mu) \cap \widehat{Z}(\mu))}{\max\{1, \text{rank}(\widehat{Z}(\mu))\}}, \quad (2.3)$$

where $\text{rank}(Z(\mu))$ is the group rank and the uniform False Discovery Rate becomes $\text{uFDR} = \mathbb{E}[\text{uFDP}]$. Here at each filtration level μ , $\text{rank}(\widehat{Z}(\mu))$ counts the number of selected group generators, namely homological features, and $\text{rank}(Z(\mu) \cap \widehat{Z}(\mu))$ counts that of correctly selected one. Our goal is to infer the homology group $\widehat{Z}(\mu)$ for all $\mu \in [\mu_0, \mu_1]$ with uFDR controlled at the given level q .

2.2 Graph Feature Selection

We start the problem with the fixed filtration level μ , which reduces the multiple hypotheses in (1.1) for the general graph features F_j . Let ψ_j be the test for $H_{0j} : F_j \not\subseteq G^*$ where $\psi_j = 1$ if we reject H_{0j} and $\psi_j = 0$ otherwise. We aim to control the false discovery rate $\text{FDR} = \mathbb{E}[\text{FDP}]$ at given level q , where $\text{FDP} = (\sum_{j \in \mathcal{H}_0} \psi_j) / (\max\{1, \sum_{j=1}^J \psi_j\})$. Here $\mathcal{H}_0 = \{1 \leq j \leq J \mid F_j \not\subseteq G^*\}$. In this paper, we propose a general multiple testing procedure to select graph features while the tail probability of FDP and the FDR can be controlled below a given level $0 < q < 1$.

The main idea of our algorithm is to use the maximum p -values to select the significant graph features. Given any graph feature F , we assign its p -value as

$$\alpha(F) = \max_{e \in E(F)} p_e. \quad (2.4)$$

Here p_e is any valid p -value for edge e . Recall that W^* is the true edge weights matrix. In the following of the entire paper, we will present our method under the general graphical model. We assume that we have a generic edge weights estimator \widehat{W} which is asymptotically normal, i.e.,

$\sqrt{n}(\widehat{W}_e - W_e^*)/\widehat{\sigma}_e \rightsquigarrow N(0, 1)$, and $\widehat{\sigma}_e^2$ is a generic estimated variance for $\sqrt{n}\widehat{W}_e$. We will present the general assumptions on these estimators in Assumption 4.1 and the concrete examples of such estimators will be discussed in Examples 2.1 and 2.2. We then can use these generic estimators to obtain the p -values under the two scenarios:

$$\begin{aligned} \text{Scenario (a): } p_e &= 2 - 2\Phi(|\sqrt{n}\widehat{W}_e/\widehat{\sigma}_e|); \\ \text{Scenario (b): } p_e &= 1 - \Phi(\sqrt{n}\widehat{W}_e/\widehat{\sigma}_e). \end{aligned} \tag{2.5}$$

Suppose we have the estimated p -values of all edges $\{p_e\}_{e \in \bar{E}}$. We begin with an initial full edge set and initialize graph feature p -values $\alpha(F_j) = 1$ for all $j \in [J]$. We then filter out edges with p -values greater than a threshold q , denoting the resulting set of edges as $E_0(q) = \{e \in \bar{E} : p_e < q\}$. We only use (2.4) to update those $\alpha(F_j)$ values for graph features F_j that can be embedded in the filtered graph $(V, E_0(q))$. Finally, we apply the Benjamini-Hochberg procedure (Benjamini and Hochberg, 1995) to the set of updated $\alpha(F_j)$ values to select the significant graph features. The Benjamini-Hochberg procedure ranks individual p -values from multiple tests and determines a threshold under which the null hypothesis can be rejected, thus controlling the FDR under q among all significant results. Throughout this paper, we refer to this method as the BHq algorithm. The detailed pseudo-code is presented in Algorithm 1.

Algorithm 1: General Graph Feature Selection with FDR Control

- 1 **Input:** Edge p -values p_e for $e \in \bar{E}$, FDR level q .
 - 2 Initialize $\alpha_j = 1$ for $j \in [J]$;
 - 3 Denote $E_0(q) = \{e \in \bar{E} : p_e < q\}$;
 - 4 **for** $F \in \{F_j : E(F_j) \subseteq E_0(q), j \in [J]\}$ **do**
 - 5 | $\alpha(F) = \max_{e \in E(F)} p_e$;
 - 6 **end**
 - 7 Order $\alpha_1, \dots, \alpha_J$ as $\alpha_{(1)} \leq \alpha_{(2)} \leq \dots \leq \alpha_{(J)}$ and set $\alpha_{(0)} = 0$;
 - 8 Let $j_{\max} = \max\{0 \leq j \leq J : \alpha_{(j)} < qj/J\}$ and $\widehat{\alpha} = q_{\max}j/J$;
 - 9 **Output:** Reject H_{0j} , i.e., $\psi_j = 1$, for those j such that $\alpha_j < \widehat{\alpha}$. Reject nothing if $j_{\max} = 0$.
-

Next we apply our general testing framework to two specific models: Gaussian graphical model and Ising model. The core is how to estimate edge weights and p -values under these two models.

2.3 Gaussian Graphical Model

Example 2.1 (Gaussian Graphical Model (GGM)). The random vector \mathbf{X} follows a multivariate Gaussian distribution $N_d(\mathbf{0}, \Sigma^*)$ with mean vector $\mathbf{0}$ and covariance matrix Σ^* . Let the precision matrix $\Theta^* = \Sigma^{*-1}$. We have $\Theta_{ij}^* = 0$ if and only if $(i, j) \notin E^*$, therefore $E^* = \{(i, j) \in V \times V \mid i \neq j, \Theta_{ij}^* \neq 0\}$.

We consider the following parameter space for precision matrices

$$\mathcal{U}(s) = \left\{ \Theta \in \mathbb{R}^{d \times d} \mid 1/\rho \leq \lambda_{\min}(\Theta) \leq \lambda_{\max}(\Theta) \leq \rho, \max_{j \in [d]} \|\Theta_{\cdot j}\|_0 \leq s, \|\Theta\|_1 \leq M, \Theta = \Theta^\top \right\}. \tag{2.6}$$

Under such parameter space, we discuss how to estimate weights and p -values for edges for the Gaussian graphical model. Given n i.i.d. observations $\mathbf{X}_1, \dots, \mathbf{X}_n$ following the distribution of \mathbf{X}

and the GLasso estimator $\widehat{\Theta}$ for Θ^* (Friedman et al., 2008). We consider the unbiased estimator $\widehat{\Theta}^d$ and its variance estimate (Neykov et al., 2018) as

$$\widehat{\Theta}_{uv}^d = \widehat{\Theta}_{uv} - \frac{\widehat{\Theta}_{\cdot u}^\top (\widehat{\Sigma} \widehat{\Theta}_{\cdot v} - \mathbf{e}_v)}{(\widehat{\Theta}_{\cdot u}^\top \widehat{\Sigma}_{\cdot u})}, \quad \widehat{\sigma}_{uv}^2 = \widehat{\Theta}_{uu}^d \widehat{\Theta}_{vv}^d + (\widehat{\Theta}_{uv}^d)^2 \quad (2.7)$$

where $\widehat{\Sigma} = 1/n \sum_{i=1}^n \mathbf{X}_i \mathbf{X}_i^\top$ is the sample covariance matrix, $\widehat{\Theta}_{\cdot j}, \widehat{\Sigma}_{\cdot j}$ is the j -th column of matrix $\widehat{\Theta}, \widehat{\Sigma}$ respectively, and $\mathbf{e}_k \in \mathbb{R}^d$ is the k -th canonical basis with only the k -th entry being 1. $\widehat{\Theta}_{uv}^d$ can be decomposed into (Neykov et al., 2019)

$$\sqrt{n}(\widehat{\Theta}_{uv}^d - \Theta_{uv}^*) = \frac{1}{\sqrt{n}} \sum_{i=1}^n \Theta_{\cdot u}^{*\top} (\mathbf{X}_i \mathbf{X}_i^\top \Theta_{\cdot v}^* - \mathbf{e}_v) + o_P(1), \quad (2.8)$$

which can be shown to be asymptotically normal, i.e., $\sqrt{n}(\widehat{\Theta}_{uv}^d - \Theta_{uv}^*) \rightsquigarrow N(0, \Theta_{uu}^* \Theta_{vv}^* + \Theta_{uv}^{*2})$.

So for Gaussian graphical model, we take $W_{uv}^* = \Theta_{uv}^*$ and $\widehat{W}_{uv} = \widehat{\Theta}_{uv}^d$. And we estimate the p -value by $p_e = 2(1 - \Phi(|\sqrt{n}\widehat{W}_e/\widehat{\sigma}_e|))$. Throughout the paper, we interchangeably use W_e and W_{uv} , Θ_e and Θ_{uv} for $e = (u, v)$. The theoretical property of \widehat{W} is presented in Proposition 4.2.

2.4 Ising Model

Example 2.2 (Ferromagnetic Ising Model). In the Ising model, $\mathbf{X} \in \{1, -1\}^d$ for each node has distribution

$$\mathbb{P}(\mathbf{X} = \mathbf{x}) = \frac{1}{Z(\mathbf{w}^*)} \exp\left(\sum_{(u,v) \in \bar{E}} w_{uv}^* x_u x_v\right), \quad (2.9)$$

where $\mathbf{x} = (x_1, \dots, x_d)^\top$ is an observation of \mathbf{X} and $Z(\mathbf{w}^*) = \sum_{\mathbf{x} \in \{1, -1\}^d} \exp\left(\sum_{(u,v) \in \bar{E}} w_{uv}^* x_u x_v\right)$ is the partition function. The Ising model is ferromagnetic in the sense that the weights $\mathbf{w}_{uv}^* \geq 0$ for all $(u, v) \in \bar{E}$.

Following Neykov and Liu (2019), we assume there is a known lower bound θ for $w_e^*, e \in E^*$ and consider the following parameter space

$$\mathcal{W} = \left\{w^* : \min_{e \in E^*} w_e^* \geq \theta, \|w^*\|_\infty \leq \Theta, \text{stanh}(\Theta) < \rho, s \geq 2\rho/(1 - \rho)\right\}, \quad (2.10)$$

where $\rho \in (0, 1)$ is a constant. For the ferromagnetic Ising model, we have $w_e^* > 0$ if and only if $e \in E^*$, and $w_e^* = 0$ for $e \notin E^*$. However, estimating the weight w_{uv}^* in the Ising model (2.9) is not easy. Lemma 3.1 in Neykov and Liu (2019) shows that the correlation between variables can be used to characterize the edge weight. Specifically, $\mathbb{E}[X_u X_v] - \tanh\theta > 0$ if and only if $w_{uv}^* > 0$. Moreover, correlation $\mathbb{E}[X_u X_v]$ is easier to estimate than w_{uv}^* . So we focus on studying the weight

$$W_{uv}^* = \mathbb{E}[X_u X_v] - \tanh(\theta). \quad (2.11)$$

Consider n i.i.d. samples $\mathbf{X}_1, \dots, \mathbf{X}_n \in \{1, -1\}^d$ from the Ising model, where $\mathbf{X}_i = (X_{i1}, X_{i2}, \dots, X_{id})^\top$. We then estimate W_{uv}^* in (2.11) and the variance by the empirical average

$$\widehat{W}_{uv} = \frac{1}{n} \sum_{i=1}^n X_{iu} X_{iv} - \tanh(\theta), \quad \widehat{\sigma}_{uv}^2 = 1 - \left(\frac{1}{n} \sum_{i=1}^n X_{iu} X_{iv}\right)^2. \quad (2.12)$$

And we estimate the p -value by $p_e = 1 - \Phi(\sqrt{n}\widehat{W}_e/\widehat{\sigma}_e)$. We have the theoretical guarantee for asymptotic normality of \widehat{W}_{uv} in Proposition 4.3.

3 Inferential Analysis for Persistent Homology

In this section, we propose the method for selecting homological features with uFDR controlled. There are two major challenges compared to the graph feature selection. First, the selected graph features could be linearly dependent in the homology group and we need to screen the independent generators among them which involves complicated algebra operators. Second, in order to estimate the persistence of graph features, it is necessary to determine the generators cross continuous filtration levels. To tackle the first issue, we apply the idea of Gram-Schmidt algorithm from linear algebra to homology group and combine it with the p -values. For the second issue, we introduce an upper-layer algorithm that efficiently identifies finite-state homology groups across the continuous filtration levels. This is to utilize the discrete structure of the graph and dynamically selecting the change point for persistent homology.

3.1 Discrete Gram-Schmidt Algorithm for Graph Homology Group

We begin by introducing the method of selecting homological features at a given filtration level μ . Similar to (2.5), we compute the p -values under the two scenarios following

$$\text{Scenario (a): } \widehat{W}_e(\mu) = |\widehat{W}_e| - \mu \text{ and } p_e(\mu) = 2 - 2\Phi(\sqrt{n}\widehat{W}_e(\mu)/\widehat{\sigma}_e);$$

$$\text{Scenario (b): } \widehat{W}_e(\mu) = \widehat{W}_e - \mu \text{ and } p_e(\mu) = 1 - \Phi(\sqrt{n}\widehat{W}_e(\mu)/\widehat{\sigma}_e).$$

The key idea of our algorithm is to keep track of a list of p -values corresponding to the selected generators in the homology group and then implement the BHq procedure. First, we choose a prior edge set E_0 , which by default considers these edges with p -values smaller than q . Let \widetilde{E} be the edge set consisting the significant generators. We initialize the algorithm with $\widetilde{E} = \emptyset$ and the list of p -values starts as empty as well. The algorithm aims to iteratively add edges from the candidate set E_0 to \widetilde{E} . In each iteration, we choose the edge (denoted as e^*) with the smallest $p_e(\mu)$ over all $e \in E_0$. After adding e^* to \widetilde{E} , we calculate the increase of the rank of the homology group of (V, \widetilde{E}) and denote it by ℓ . The algorithm to compute the rank of the homology group has been well established in the literature and it is computationally efficient with linear complexity to the number of simplices (Fugacci et al., 2016). We then add ℓ repetitions of $p_{e^*}(\mu)$ into the p -value list. This can be interpreted as a discrete Gram-Schmidt procedure by adding the p -values for the ℓ generators independent to the selected generators in the previous iteration. Compared to the Gram-Schmidt algorithm in the linear algebra, our method does not need to explicitly find the induced generators but simply add $p_{e^*}(\mu)$ for ℓ times. We only need to identify the rank without selecting specific generators which makes our approach computationally efficient. The algorithm stops when the candidate set E_0 becomes empty. The last step is to apply the BHq procedure on the p -value list and obtain a p -value threshold $\widehat{\alpha}$ with the selected edge set $\widehat{E}(\mu) = \{e \in E_0 : p_e(\mu) < \widehat{\alpha}\}$ and the selected homology group $\widehat{Z}(\mu) = Z(\widehat{E}(\mu))$. The detailed algorithm is presented in Algorithm 2.

Algorithm 2: Discrete Gram-Schmidt (DGS) Algorithm

```

1 Function DGS( $\mu$ )
2 Input: Filtration level  $\mu$ , FDR level  $q$ .
3 Initialize  $\tilde{E} = \emptyset$ ,  $E_0 = \{e \in \tilde{E} : p_e(\mu) < q\}$  and  $j = 0$ ;
4 while  $E_0 \neq \emptyset$  do
5   Denote  $e^* = \arg \min_{e \in E_0} p_e(\mu)$ ;
6   Calculate the increased rank  $\ell = \text{rank}(Z(\{e^*\} \cup \tilde{E})) - \text{rank}(Z(\tilde{E}))$ ;
7   if  $\ell > 0$  then
8     Assign  $p$ -values to the  $\ell$  generators  $\alpha_i = p_{e^*}(\mu)$  for  $i = j + 1, \dots, j + \ell$ ;
9      $j = j + \ell$ ;
10  end
11   $\tilde{E} = \tilde{E} \cup \{e^*\}$ ,  $E_0 = E_0 \setminus \{e^*\}$ ;
12 end
13 Set  $\alpha_{(0)} = 0$  and let  $j_{\max} = \max\{0 \leq i \leq j : \alpha_{(i)} \leq qi/\bar{J}\}$ ,  $\hat{\alpha} = qj_{\max}/\bar{J}$ ;
14 Output: Selected edge set  $\hat{E}(\mu) = \{e \in \tilde{E} : p_e(\mu) < \hat{\alpha}\}$  and the selected homology group
     $\hat{Z}(\mu) = Z(\hat{E}(\mu))$ .
  
```

3.2 KHAN Algorithm: FDR Selection for the Persistent Homology

To obtain the uniform selection for persistent homology over continuous filtration line $\mu \in [\mu_0, \mu_1]$, instead of applying Algorithm 2 point by point for infinite number of μ 's, the key idea of the KHAN algorithm is to identify the finite change points of the barcode and apply the discrete Gram-Schmidt algorithm at each change point.

We initialize the edge set and its homology group estimator at the minimum filtration level as $E^{(0)} = \hat{E}(\mu_0)$ and $\hat{Z}^{(0)} = \hat{Z}(\mu_0)$ applying the discrete Gram-Schmidt algorithm. We then iteratively identify the next change point by estimate the confidence lower bound for the edge weights. In specific, suppose at the t -th iteration, we have the estimated edge set $E^{(t)}$ and the homology group $\hat{Z}^{(t)}$. We update the next change point under two scenarios as

$$\begin{aligned}
 \text{Scenario (a): } \mu^{(t+1)} &= \min\left\{|\widehat{W}_e| - \Phi^{-1}(1 - \alpha)\widehat{\sigma}_e/\sqrt{n} : e \in E^{(t)}\right\}, & \alpha &= q \text{rank}(\hat{Z}^{(t)})/(2\bar{J}), \\
 \text{Scenario (b): } \mu^{(t+1)} &= \min\left\{\widehat{W}_e - \Phi^{-1}(1 - \alpha)\widehat{\sigma}_e/\sqrt{n} : e \in E^{(t)}\right\}, & \alpha &= q \text{rank}(\hat{Z}^{(t)})/\bar{J},
 \end{aligned} \tag{3.1}$$

where $\bar{J} = \text{rank}(Z(\tilde{E}))$ whose order is studied in Proposition E.1 of the Supplementary Material. Recall that \widehat{W}_e and $\widehat{\sigma}_e^2$ are the generic weights and variance estimators and their examples under Gaussian graphical models and Ising models can be found in Sections 2.3 and 2.4. We then update the edge set $E^{(t+1)} = \hat{E}(\mu^{(t+1)})$ and the homology group $\hat{Z}^{(t+1)} = \hat{Z}(\mu^{(t+1)})$ by the discrete Gram-Schmidt algorithm. Then we can interpolate the persistent homology group estimator $\hat{Z}(\mu) = \hat{Z}(\mu^{(t)})$ for all $\mu \in [\mu^{(t)}, \mu^{(t+1)})$. We repeat the process until $\mu^{(t+1)} > \mu_1$. If $\mu_1 = \infty$, we stop the algorithm when the estimated homology group becomes empty. The detailed KHAN algorithm is presented in Algorithm 3. See Figure 2 for the illustration of the procedure. The algorithm is computationally efficient as the maximum number of iterations is $|E^{(0)}|$ and the implementation of discrete Gram-Schmidt only involves rank computation without basis selection.

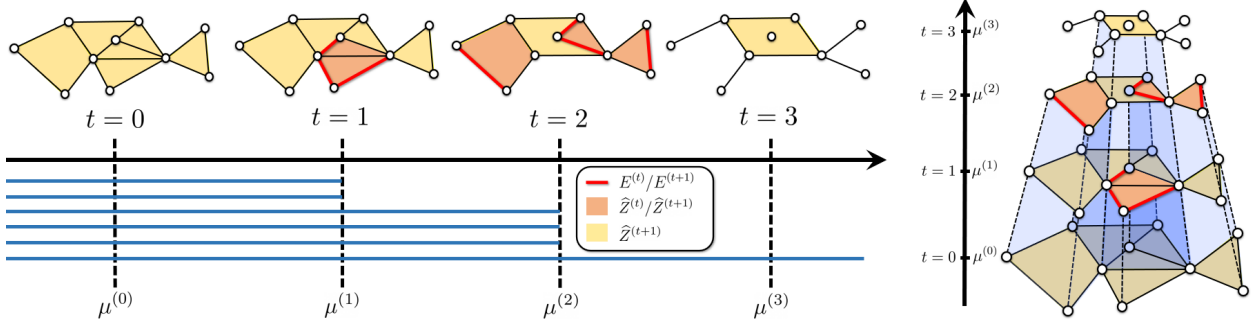


Figure 2: (Left) Illustration of the method of selecting homological features for persistent homology. At each iteration t , all the edges on the graph make the filtered edge set $E^{(t)}$, the weight of the red edge(s) represents the next filtration level $\mu^{(t+1)}$, the yellow cycles represent the remaining generator(s) in the next iteration, and the orange cycle(s) represents the disappearing generator(s) in the next iteration. The blue horizontal lines represent the life time of each cycle along the filtration of graph. (Right) Illustrations in 3D of the filtration of graphs when the filtration level μ increases.

Algorithm 3: KHAN: **K**-Dimensional Persistent **H**omology **A**daptive Selection **N** Algorithm

- 1 **Input:** Estimated edge weights $\{\widehat{W}_e\}_{e \in \widehat{E}}$, FDR level q .
 - 2 Initialize $t = 0$, edge set and homology group at level μ_0 as $E^{(0)} = \widehat{E}(\mu_0)$ and $\widehat{Z}^{(0)} = \widehat{Z}(\mu_0)$ applying DGS(μ_0) in Algorithm 2 ;
 - 3 **while** $\widehat{Z}^{(t)} \neq \emptyset$ **do**
 - 4 Determine the next change point using (3.1);
 - 5 Update the edge set $E^{(t+1)} = \widehat{E}(\mu^{(t+1)})$ and the homology group $\widehat{Z}^{(t+1)} = \widehat{Z}(\mu^{(t+1)})$ by applying DGS($\mu^{(t+1)}$) ;
 - 6 $t = t + 1$;
 - 7 **end**
 - 8 **Output:** $\widehat{Z}(\mu) = \widehat{Z}^{(s)}$ for $\mu \in [\mu^{(s)}, \mu^{(s+1)})$ and $\widehat{Z}(\mu_0) = \widehat{Z}^{(0)}$, $\widehat{Z}(\mu) = \emptyset$ if $\mu > \mu^{(t)}$.
-

4 Theoretical Results

In this section, we provide the theoretical results for the graph feature selection algorithm proposed in Section 2, and persistent homology selection algorithms proposed in Section 3.

4.1 Graph Feature Selection

To ensure the FDR is adequately controlled in the multiple testing problem (1.1) for general graphical models, it we need to impose assumptions for the generic estimator \widehat{W}_e and $\widehat{\sigma}_e$. In specific, we need the following assumption on the asymptotic normality of \widehat{W}_e and the consistency of the variance estimator $\widehat{\sigma}_e$.

Assumption 4.1. For some constant $C > 0$, there exist i.i.d. random variables $\xi_i(e)$ for $i = 1, 2, \dots, n$ with bounded ψ_1 -orlicz norm and $W_e = \sum_{i=1}^n \xi_i(e)/n$ such that

$$\sup_{e \in \bar{E}} \left(\frac{\sqrt{n} |\widehat{W}_e - W_e - W_e^*|}{\sigma_e \sqrt{\log d}} + \left| \frac{\sigma_e}{\widehat{\sigma}_e} - 1 \right| \right) \leq \frac{C}{\log d} + o_P(1),$$

where $\sigma_e^2 = \text{Var}(\xi_1(e))$.

The assumption imposes that \widehat{W}_e can be decomposed into three parts: (1) the dominating error term W_e , which is asymptotically normal; (2) W_e^* , the true edge weight; and (3) the remainder term, which is at the order of $1/\sqrt{n \log d}$. Such decomposition has been achieved under different graphical models (Van de Geer et al., 2014; Neykov and Liu, 2019). Next we provide two examples of edge weight estimators \widehat{W}_e satisfying Assumption 4.1 under the Gaussian graphical model and the Ising model.

Recall that in Section 2.3, the Gaussian graphical model use the precision matrix as the weight $W_{uv}^* = \Theta_{uv}^*$ and estimated by $\widehat{W}_{uv} = \widehat{\Theta}_{uv}^d$ in (2.7). By (2.8), the dominating error term W_{uv} becomes

$$W_{uv} = \frac{1}{n} \sum_{i=1}^n \Theta_{u \cdot}^* (\mathbf{X}_i \mathbf{X}_i^\top \Theta_{\cdot v}^* - \mathbf{e}_v). \quad (4.1)$$

We have the following proposition that validates Assumption 4.1 under the Gaussian graphical model. The proof of this proposition is deferred to Section D.1 in the Supplementary Material.

Proposition 4.2. For GGM with parameter space $\Theta \in \mathcal{U}(s)$ defined in (2.6), suppose $s^2 \log^4(dn)/n = o(1)$, the estimator \widehat{W}_e and $\widehat{\sigma}_e^2$ defined in (2.7) with W_{uv} in (4.1) satisfy Assumption 4.1.

For the case of Ising model introduced in Section 2.4. Recall that we consider the weight $W_{uv}^* = \mathbb{E}[X_u X_v] - \tanh(\theta)$ and its estimator \widehat{W}_{uv} in (2.12). Then the dominating error term becomes

$$W_{uv} = \frac{1}{n} \sum_{i=1}^n X_{iu} X_{iv} - \mathbb{E}[X_u X_v]. \quad (4.2)$$

We have the following theoretical guarantee for asymptotic normality of \widehat{W}_{uv} . The proof of this proposition is left to Section D.2 in the Supplementary Material.

Proposition 4.3. For the Ising models in (2.9) with the parameter space defined in (2.10), the estimator \widehat{W}_e and $\widehat{\sigma}_e^2$ defined in (2.12) with W_{uv} in (4.2) satisfy Assumption 4.1.

We next introduce the signal strength condition required for our theoretical analysis. This condition helps to identify the subset of hypotheses with sufficiently strong signals within the context of graph feature selection. Specifically, we define the set of hypotheses with strong signal strength under the two scenarios as

$$\begin{aligned} \text{Scenario (a): } \widetilde{\mathcal{H}}_1 &= \left\{ j \in \mathcal{H}_1 : \min_{e \in E(F_j)} |W_e^*| \geq C \sqrt{\log d/n} \right\}; \\ \text{Scenario (b): } \widetilde{\mathcal{H}}_1 &= \left\{ j \in \mathcal{H}_1 : \min_{e \in E(F_j)} W_e^* \geq C \sqrt{\log d/n} \right\}. \end{aligned} \quad (4.3)$$

To characterize the dependence among the multiple tests in (1.1), we introduce

$$N_j = \{e \in E(F_j) : W_e^* = 0\}, \text{ for } j = 1, 2, \dots, J, \quad (4.4)$$

which is the null edge set for the structure F_j in the graph G^* . Recall that $\xi_i(e)$ is the summand of $W_e = \sum_{i=1}^n \xi_i(e)/n$ defined in Assumption 4.1. We define the dependence level as

$$S = |\{(j_1, j_2) : j_1, j_2 \in \mathcal{H}_0, j_1 \neq j_2, \exists e_1 \in N_{j_1}, e_2 \in N_{j_2}, \text{ s.t. } |\text{Cov}(\xi_1(e_1), \xi_1(e_2))| \geq C(\log d)^{-2}(\log \log d)^{-1}\}|, \quad (4.5)$$

where C is a sufficiently large constant. The dependence level quantifies the dependency among multiple hypotheses by the number of graph feature pairs F_{j_1}, F_{j_2} whose null edges covariances are larger than certain level.

Next we present the assumption on the scaling conditions among the number of hypotheses and the the dependence level S . Recall that $\mathcal{H}_0 = \{1 \leq j \leq J \mid F_j \not\subseteq G^*\}$, $\mathcal{H}_1 = \{1 \leq j \leq J \mid F_j \subseteq G^*\}$ and $\tilde{\mathcal{H}}_1 \subseteq \mathcal{H}_1$ is defined in (4.3). We assume the following condition.

Assumption 4.4 (Signal strength and dependence conditions). We assume

$$\underbrace{\frac{J}{|\mathcal{H}_0| \cdot |\tilde{\mathcal{H}}_1|}}_{\text{Signal strength}} + \underbrace{\frac{JS}{|\mathcal{H}_0|^2 |\tilde{\mathcal{H}}_1|}}_{\text{Dependence effect}} = o\left(\frac{1}{\log d}\right).$$

Assumption 4.4 comprises two types conditions. The first condition involves the numbers of null hypotheses and the alternatives with strong enough signal strength. In specific, if the number of the null hypotheses $|\mathcal{H}_0|$ is of the same order of J , then it suffices to validate the first condition when the number of alternatives with strong signals has $|\tilde{\mathcal{H}}_1| = \omega(\log d)$. The second condition balances the dependence level and the number of hypotheses. Again, if $|\mathcal{H}_0| \asymp J$, the second term is satisfied when $S = o(|\mathcal{H}_0| \cdot |\tilde{\mathcal{H}}_1|/\log d)$. Similar assumption is also imposed by Zhang and Lu (2024), but our assumption is weaker as we only take into account the edges pairs whose covariance is significantly large in (4.5) but Eq.(5.3) in Zhang and Lu (2024) counts any non-zero covariance which makes their dependence level significantly larger. In the following, we will show that such condition can be validated for a wide range of graphs under the Gaussian graphical model and the Ising model. We denote $M = \max_j |V(F_j)|$ as the maximum size of the graph features of interest and we can give an explicit upper bound on S to simplify the second condition into a direct sufficient condition on $|\tilde{\mathcal{H}}_1|$.

Proposition 4.5. For the Gaussian graphical model with the weights $\Theta \in \mathcal{U}(s)$ where s is the maximum degree of the graph G^* , we have $S = O(|\mathcal{H}_0|d^{M-2}s^2)$.

The proof is deferred to Section D.3 in the Supplementary Material. As $M = \max_j |V(F_j)|$, then the maximal possible number of tests $J = |\mathcal{H}_0| + |\mathcal{H}_1| \asymp d^M$. By Proposition 4.5, under GGM, if the number of null hypotheses is balanced with the alternatives, i.e., $|\mathcal{H}_0| \asymp |\mathcal{H}_1| \asymp d^M$, then the dependence effect in Assumption 4.4 can be implied when $|\tilde{\mathcal{H}}_1| = \omega(s^2 d^{M-2} \log d)$.

The following proposition provides an upper bound of S under the Ising model.

Proposition 4.6. For ferromagnetic Ising models, assume that the graph with d nodes consists of d/s trees and each tree has s nodes. We have $S = O(|\mathcal{H}_0|d^{M-1}s)$.

The proof is deferred to Section D.4 in the Supplementary Material. Similarly, under the conditions of Proposition 4.6, if $|\mathcal{H}_0| \asymp |\mathcal{H}_1|$, the dependence effect can be implied when $|\tilde{\mathcal{H}}_1| = \omega(sd^{M-1} \log d)$.

4.1.1 Theoretical Results for Graph Feature Selection

The following theorem shows that Algorithm 1 can control the FDR of graph feature selection.

Theorem 4.7 (General FDR control). Suppose $\log d/\log n = O(1)$. Under Assumptions 4.1 and 4.4, we have that the $\{\psi_j\}_{j \in [J]}$ determined by Algorithm 1 satisfies

$$\text{FDP} \leq q \frac{|\mathcal{H}_0|}{J} + o_P(1), \quad \text{FDR} \leq q \frac{|\mathcal{H}_0|}{J} + o(1).$$

The proof of this theorem is deferred to Section B.1 in the Supplementary Material. On the other side, the next theorem shows that the algorithm is also powerful.

Theorem 4.8 (Power Analysis). For $\{\psi_j\}_{j \in [J]}$ determined by Algorithm 1, under the same conditions of Theorem 4.7, we have

$$\mathbb{P}(\psi_j = 1, \text{ for all } j \in \tilde{\mathcal{H}}_1) = 1 - o(1),$$

where $\tilde{\mathcal{H}}_1$ is defined in (4.3).

This theorem guarantees that the true alternative hypotheses satisfying certain signal strength condition will be selected with probability going to 1. The proof of this theorem can be found in Section B.2 in the Supplementary Material. We have the following corollaries for the above general results under the Gaussian and Ising graphical models. The proofs are postponed to Sections D.6 and D.7 in the Supplementary Material.

Corollary 4.9 (Graph feature selection under GGM). Under the same conditions of Proposition 4.2, if $\log d/\log n = O(1)$ and Assumption 4.4 is satisfied, we have

$$\text{FDP} \leq q \frac{|\mathcal{H}_0|}{J} + o_P(1), \quad \text{FDR} \leq q \frac{|\mathcal{H}_0|}{J} + o(1),$$

and the uniform power control

$$\mathbb{P}(\psi_j = 1, \text{ for all } j \in \tilde{\mathcal{H}}_1) = 1 - o(1).$$

Corollary 4.10 (Graph feature selection under Ising models). Under the same conditions of Proposition 4.3, if $\log d/\log n = O(1)$ and Assumption 4.4 is satisfied, we have

$$\text{FDP} \leq q \frac{|\mathcal{H}_0|}{J} + o_P(1), \quad \text{FDR} \leq q \frac{|\mathcal{H}_0|}{J} + o(1),$$

and the uniform power control

$$\mathbb{P}(\psi_j = 1, \text{ for all } j \in \tilde{\mathcal{H}}_1) = 1 - o(1).$$

4.2 Theoretical Results for Persistent Homology

In this section, we provide the theoretical justification of the proposed KHAN algorithm. Similar to the dependence level S in Assumption 4.4, we need to quantify the dependency among different homological features at different filtration levels. We first introduce the concept of critical edges which may change the rank of the homology group. Let the edges in \bar{E} be ordered as $e_{(1)}, e_{(2)}, \dots, e_{(|\bar{E}|)}$ such that $W_{e_{(1)}}^* \geq \dots \geq W_{e_{(|\bar{E}|)}}^*$ and denote $E_{(i)} = \{e_{(1)}, \dots, e_{(i)}\}$ for all $i \in [|\bar{E}|]$ and $E_{(0)} = \emptyset$. Recall that $\bar{J} = \text{rank}(Z(\bar{E}))$. To characterize the critical edges which may increase the rank in Algorithm 2, we construct the critical edge list $\bar{e}_1, \dots, \bar{e}_{\bar{J}}$ by the following procedure. Let $\ell_i = \text{rank}(Z(E_{(i)})) - \text{rank}(Z(E_{(i-1)}))$ for all $i \in [|\bar{E}|]$. Then the j -th critical edge $\bar{e}_j = e_{(i)}$ if j has $\sum_{u=1}^{i-1} \ell_u < j \leq \sum_{u=1}^i \ell_u$. We then define the dependence level at the filtration level μ by

$$\bar{S}(\mu) = \left| \left\{ (j_1, j_2) : j_1 \neq j_2, \bar{e}_{j_1}, \bar{e}_{j_2} \notin E^*(\mu), |\text{Cov}(\xi_1(\bar{e}_{j_1}), \xi_1(\bar{e}_{j_2}))| \geq \frac{C}{(\log d)^2 \log(\log d)} \right\} \right|, \quad (4.6)$$

Similar to (4.5), $\bar{S}(\mu)$ characterizes the dependence between the pair of critical edges $(\bar{e}_{j_1}, \bar{e}_{j_2})$.

Similar to Assumption 4.4, we need to impose the assumption on the scaling conditions of the number of hypotheses and dependence level. However, as the generators could be linearly dependant among each other in the homology group, the homological features in (1.2) are not as identifiable as the graph features in (1.1). Therefore, we bypass the identifiability issue by defining the uFDP in (2.3) through the identifiable rank difference instead of listing the null hypotheses explicitly. Following this idea, given any filtration level $\mu \in [\mu_0, \mu_1]$, we define the number of significant alternatives $|\tilde{\mathcal{H}}_1(\mu)| = \text{rank}(Z(\mu + C\sqrt{\log d/n}))$ and the number of null hypotheses $|\bar{\mathcal{H}}_0(\mu)| = \bar{J} - \text{rank}(Z(\mu))$. Here we use the notation of cardinality without introducing the set simply in order to link the notations to the ones in Assumption 4.4. We refer to Section C in the Supplementary Material for a detailed discussion on the definitions above.

Assumption 4.11. For a sufficiently large constant C , we assume

$$\underbrace{\frac{\bar{J}}{|\bar{\mathcal{H}}_0(\mu_1)| \cdot |\tilde{\mathcal{H}}_1(\mu_1)|}}_{\text{Signal strength}} + \underbrace{\frac{\bar{J}\bar{S}(\mu_1)}{|\bar{\mathcal{H}}_0(\mu_1)|^2 |\tilde{\mathcal{H}}_1(\mu_1)|}}_{\text{Dependence effect}} = o\left(\frac{1}{\log d}\right).$$

Notice that it is sufficient to assume Assumption 4.11 only for $\mu = \mu_1$ without the uniform control on $\mu \in [\mu_0, \mu_1]$. This makes the assumption less stringent and easier to verify. We have the following proposition to bound $\bar{S}(\mu)$ under the Gaussian graphical model and the Ising model. The proof is deferred to Section D.5 in the Supplementary Material.

Proposition 4.12. Define $R = \max_{i=1}^{|\bar{E}|} \ell_i$ as the maximal increased rank. For the Gaussian graphical model with $s(\mu)$ being the maximum degree of graph $G^*(\mu)$, we have

$$\bar{S}(\mu) = O(|\bar{\mathcal{H}}_0(\mu)| \cdot s(\mu)^2 R).$$

For the ferromagnetic Ising model, assuming that the graph $G^*(\mu)$ with d nodes consists of $d/s(\mu)$ trees, with each tree having $s(\mu)$ nodes, we have

$$\bar{S}(\mu) = O(|\bar{\mathcal{H}}_0(\mu)| \cdot s(\mu)dR).$$

Based on Proposition 4.12, under the Gaussian graphical model, it suffices to verify Assumption 4.11 if the number of strong signals $|\tilde{\mathcal{H}}_1(\mu_1)| = \omega(Rs(\mu_1)^2 \log d)$. Under the Ising model, Assumption 4.11 can be implied by $|\tilde{\mathcal{H}}_1(\mu_1)| = \omega(Rs(\mu_1)d \log d)$.

The following theorem controls the uFDP in (2.3) for the KHAN algorithm. The proofs can be found in Section C in the Supplementary Material.

Theorem 4.13 (uFDR and Power of KHAN). Suppose $\log d / \log n = O(1)$ and Assumptions 4.1 and 4.11 are satisfied. Algorithm 3 has

$$\text{uFDP} \leq q|\mathcal{H}_0(\mu_1)|/\bar{J} + o_P(1), \quad \text{uFDR} \leq q|\mathcal{H}_0(\mu_1)|/\bar{J} + o(1).$$

We also have the uniform power of the selections

$$\mathbb{P}\left(Z(\mu + C\sqrt{\log d/n}) \subseteq \hat{Z}(\mu) \text{ for all } \mu \in [\mu_0, \mu_1]\right) = 1 - o(1).$$

We have the following corollaries under the Gaussian graphical model and the Ising model.

Corollary 4.14. Suppose Assumption 4.11 is satisfied and $\log d / \log n = O(1)$. For Gaussian graphical model with $\Theta^* \in \mathcal{U}(s)$, we further assume $s^2 \log^4(dn)/n = o(1)$, then Algorithm 3 satisfies

$$\text{uFDP} \leq q + o_P(1), \quad \text{uFDR} \leq q + o(1).$$

and the uniform power control

$$\mathbb{P}\left(Z(\mu + C\sqrt{\log d/n}) \subseteq \hat{Z}(\mu) \text{ for all } \mu \in (\mu_0, \mu_1)\right) = 1 - o(1).$$

Corollary 4.15. Suppose Assumption 4.11 is satisfied and $\log d / \log n = O(1)$. For Ising models with $w^* \in \mathcal{W}$, Algorithm 3 satisfies

$$\text{uFDP} \leq q + o_P(1), \quad \text{uFDR} \leq q + o(1),$$

and the uniform power control

$$\mathbb{P}\left(Z(\mu + C\sqrt{\log d/n}) \subseteq \hat{Z}(\mu) \text{ for all } \mu \in (\mu_0, \mu_1)\right) = 1 - o(1).$$

The proofs can be found in Section D.8 in the Supplementary Material.

5 Application to SARS-CoV-2 Spike Protein Data

The COVID-19 pandemic has had a devastating impact worldwide. Infection by the causative agent, severe acute respiratory syndrome coronavirus 2 (SARS-CoV-2) involves the attachment of the receptor-binding domain (RBD) of its spike proteins to the ACE2 receptors on the peripheral membrane of host cells (Ou et al., 2020). The binding process begins with a conformational change in the spike protein, transitioning from a downward orientation to an upward orientation, thereby exposing the RBD to the receptor. Recent studies that search for therapeutics have primarily focused on the RBD that is highly prone to mutations. However, it is worth considering that other residues within the spike protein, apart from the RBD, could also be potential targets for

inhibition (Liu et al., 2020). To explore this possibility, we apply our method to identify these potential target residues based on persistent homology, taking into account the protein’s complex network structure.

We use the trajectory data from (Ray et al., 2021). The data encompasses three distinct states of the SARS-CoV-2 spike protein: closed, partially open, and fully open. The protein consists of three chains, with each chain comprising 1146 residues and four domains: N-terminal domain (NTD), RBD, linker, and S2. At a fundamental level, conformational changes in protein structure originate from intricate combinations of transitions between different states of the protein backbone’s torsional angles, specifically ϕ and ψ , which are used as features of the residues. Additionally, 173 features of pairwise distances for residues from the RBD are provided, which are calculated between them and from other parts of the spike near the RBD. These distance features capture the down-to-up transition of the RBD, and residues are identified to be important for the conformational change if their backbone torsion angles are highly correlated to these features. In total, we obtain $d = 7048$ features consisting of backbone torsion angles and distances, with the sample sizes n of 8497, 14888, 8131 for the closed, partially open, and fully open states, respectively. We build a d -dimensional Gaussian graphical model for each state to analyze the relationship among these features simultaneously, to gain insights into the specific residues that have essential functions in the infection process. We convert the angle features by the transform $\Phi^{-1}(\widehat{P}_j(\cdot))$, where $\widehat{P}_j(\cdot)$ denotes the empirical distribution of the j -th angle feature.

During each stage, residues exhibiting strong connections with numerous other residues can be considered as crucial. Specifically, we apply the proposed persistent homology selection algorithm to obtain the evolution of homology groups among the features. In order to evaluate the importance of the selected homological features, we define the importance score of each feature as the length of the filtration interval of each feature exists. Then, the importance score of each residue is calculated by summing over the importance scores of all the homological features containing the residue. The detailed algorithm for determining the importance scores is presented in Algorithm 4 in the Supplementary Material.

A subset of residues outside the RBD can exert significant influence on the conformational changes of the spike protein, thereby impacting viral infection. Specifically, residues located in the linker domain connecting the RBD and the S2 domain act as a pivotal hinge, facilitating the transition of the RBD from a downward to an upward position through torsional changes in the protein backbone. Residues within the S2 domain or the NTD play a crucial role in modulating the dynamics of the RBD or linker domain, owing to their spatial proximity to the RBD in the three-dimensional conformation. These phenomenon has been previously elucidated in (Ray et al., 2021).

To provide a more intuitive demonstration of the significant impact of residues from other domains on the RBD, we initially select 100 homological features from each stage based on their edge weights and constructed graphs accordingly. By visualizing the graphs from the three stages as Figure 3A, it is illustrated that the yellow nodes representing residues from the RBD exhibit strong connectivity with residues from other domains. This phenomenon is further evident in Figure 3B, which is generated from the correlation analysis between residues within the RBD and residues located in other regions. Figure 3B demonstrates the strong associations and dependencies between these residues. In particular, there exists a significant correlation between residues originating from the RBD and residues located in the NTD, the linker domain, as well as a subset of residues within the S2 domain.

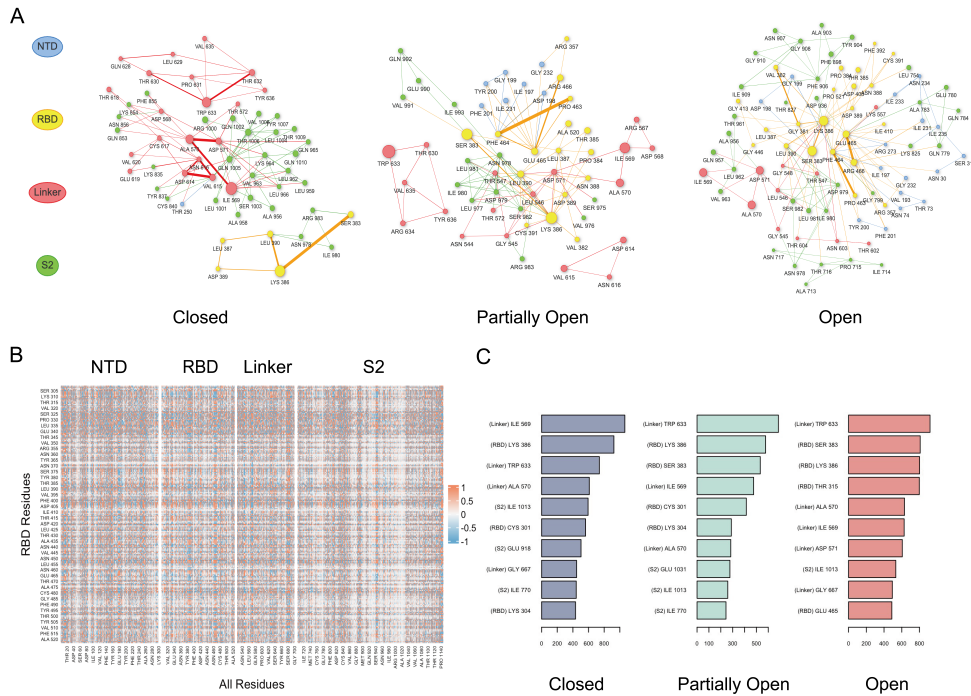


Figure 3: This figure presents a comprehensive visualization of the connectivity and correlation analysis among residues across different domains. Panel A highlights the strong connectivity of residues from the RBD (the yellow nodes) with those from other domains. Panel B showcases the correlation analysis, emphasizing the strong associations between residues within the RBD and those in the NTD, the linker domain, and a portion of the S2 domain. Panel C summarizes the top 10 residues identified at each stage based on their importance scores.

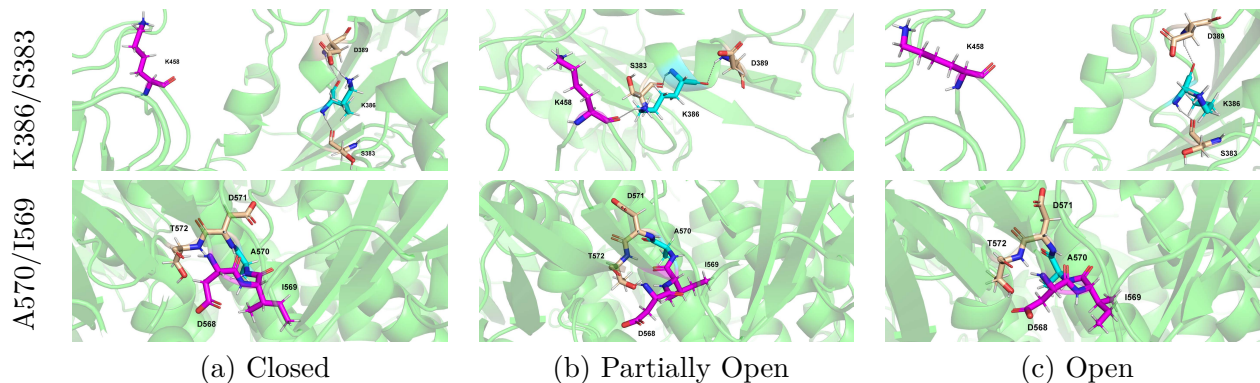


Figure 4: Illustration of the conformational changes and disruption of hydrogen bonds in residues K386/S683 and A570/I569 across three stages.

At each stage, we pick the top 10 residues in terms of the important score, which are summarized in Figure 3C. Our method successfully identifies the residues previously reported in (Ray et al., 2021), such as A570 and I569, confirming the effectiveness of our approach. Additionally, our method discovers novel residues that were not reported in (Ray et al., 2021), primarily located in the linker and S2 domains.

For a more comprehensive analysis, we have illustrated the snapshots of residues K386/S683 and A570/I569 in Figure 4. These snapshots reveal the disruption of hydrogen bonds and notable conformational changes between the three stages, emphasizing the significance of these residues in our investigation. Moreover, we have indicated the location of these residues in the protein structure, as depicted in Figure 5, revealing their close proximity to the RBD. The spatial arrangement of these residues in the 3D structure demonstrates their potential influence on the dynamics of the RBD. This observation further strengthens the validity of our findings.

Finally, we present the number of residues with non-zero important scores for each domain at each state in Figure 6. It shows that a substantial majority of residues are attributed to the S2 domain. However, as the filtration level gradually increases, there is a substantial reduction in residues originating from the S2 domain. In contrast, residues derived from the linker domain and RBD manifest a more gradual decrease, indicative of a higher level of persistence. These observations lend further support to our aforementioned findings.

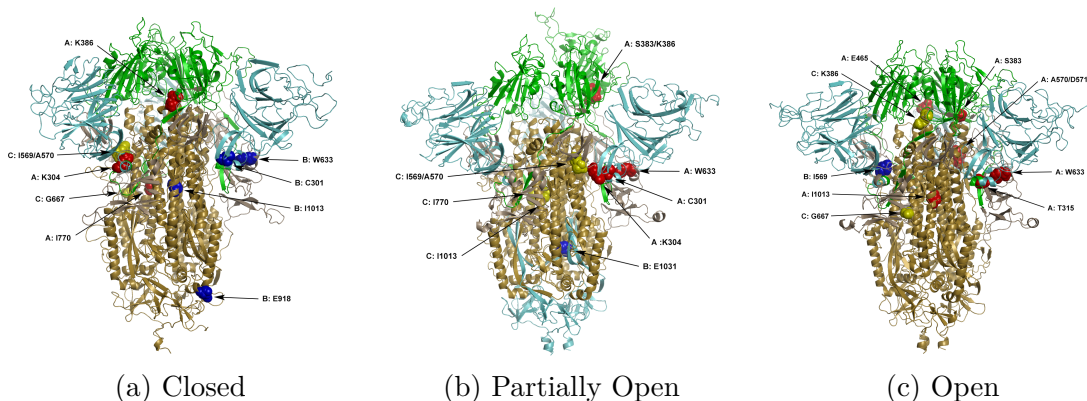


Figure 5: Visualization of the location of residues within the protein structure, emphasizing their proximity to the RBD. Color coding: Chain A in red, Chain B in blue, Chain C in yellow. Domains are distinguished as follows: NTD in light blue, RBD in green, the linker domain in grey, and the S2 domain in khaki.

6 Conclusion

This paper presents a flexible and general approach for the simultaneous detection of graph features with false discovery rate controlled. We also propose to select homological features from persistent homology with uniform false discovery rate controlled. Our method eliminates the need for maximal statistics and bootstrap for multiplicity control, making it simpler and faster than existing methods for simultaneous combinatorial inference.

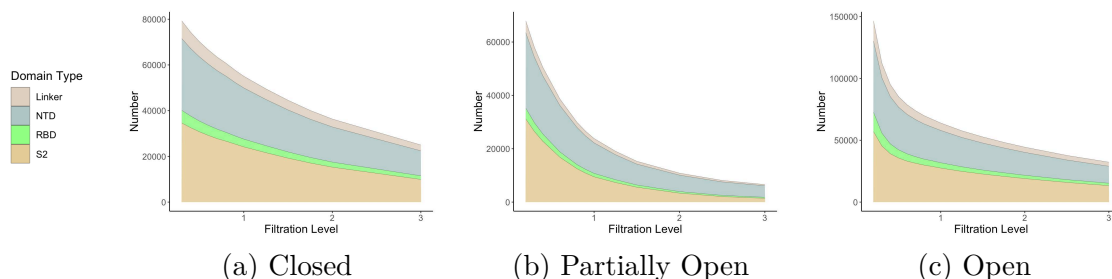


Figure 6: The number of residues with non-zero important scores for each domain at each state.

References

- AKTAS, M. E., AKBAS, E. and FATMAOUI, A. E. (2019). Persistence homology of networks: methods and applications. *Applied Network Science* **4** 1–28.
- BASSETT, D. S. and SPORNS, O. (2017). Network neuroscience. *Nature Neuroscience* **20** 353–364.
- BENJAMINI, Y. (2010). Discovering the false discovery rate. *Journal of the Royal Statistical Society Series B: Statistical Methodology* **72** 405–416.
- BENJAMINI, Y. and HOCHBERG, Y. (1995). Controlling the false discovery rate: a practical and powerful approach to multiple testing. *Journal of the Royal Statistical Society: Series B (Methodological)* **57** 289–300.
- BHATTACHARYA, B. B. and MUKHERJEE, S. (2018). Inference in ising models. *Bernoulli* **24** 493–525.
- CAI, T., LIU, W. and LUO, X. (2011). A constrained l1 minimization approach to sparse precision matrix estimation. *Journal of the American Statistical Association* **106** 594–607.
- CAI, T. T., LIU, W. and ZHOU, H. H. (2016). Estimating sparse precision matrix: Optimal rates of convergence and adaptive estimation. *The Annals of Statistics* 455–488.
- CAI, T. T. and MA, Z. (2013). Optimal hypothesis testing for high dimensional covariance matrices. *Bernoulli* **19** 2359–2388.
- CAI, T. T. and ZHANG, A. (2016). Inference for high-dimensional differential correlation matrices. *Journal of Multivariate Analysis* **143** 107–126.
- CHEN, M., REN, Z., ZHAO, H. and ZHOU, H. (2016). Asymptotically normal and efficient estimation of covariate-adjusted gaussian graphical model. *Journal of the American Statistical Association* **111** 394–406.
- CLARK, D. P. and PAZDERNIK, N. J. (2013). Molecular biology. Second edition ed. Academic Press, Boston.
- COUNCIL, N. R. ET AL. (2002). Acute exposure guideline levels for selected airborne chemicals: Volume 2. *National Academies Press (US)*.
- DING, X. and ZHOU, Z. (2020). Estimation and inference for precision matrices of nonstationary time series. *The Annals of Statistics* **48** 2455–2477.
- EVANS, R., O’NEILL, M., PRITZEL, A., ANTROPOVA, N., SENIOR, A. W., GREEN, T., ŽÍDEK, A., BATES, R., BLACKWELL, S., YIM, J. ET AL. (2021). Protein complex prediction with AlphaFold-Multimer. *BioRxiv*.
- FAN, J., LIAO, Y. and LIU, H. (2016). An overview of the estimation of large covariance and precision matrices. *The Econometrics Journal* **19** C1–C32.
- FASY, B. T., LECCI, F., RINALDO, A., WASSERMAN, L., BALAKRISHNAN, S. and SINGH, A. (2014). Confidence sets for persistence diagrams. *The Annals of Statistics* **42** 2301 – 2339.
- FRIED, J. R. (2014). *Polymer science and technology*. Pearson Education.
- FRIEDMAN, J., HASTIE, T. and TIBSHIRANI, R. (2008). Sparse inverse covariance estimation with the graphical lasso. *Biostatistics* **9** 432–441.
- FUGACCI, U., SCARAMUCCIA, S., IURICICH, F., DE FLORIANI, L. ET AL. (2016). Persistent homology: a

- step-by-step introduction for newcomers. In *STAG*.
- GHRIST, R. (2008). Barcodes: the persistent topology of data. *Bulletin of the American Mathematical Society* **45** 61–75.
- HORAK, D., MALETIĆ, S. and RAJKOVIĆ, M. (2009). Persistent homology of complex networks. *Journal of Statistical Mechanics: Theory and Experiment* **2009** P03034.
- ILYAS, M. U., SHAFIQ, M. Z., LIU, A. X. and RADHA, H. (2011). A distributed and privacy preserving algorithm for identifying information hubs in social networks. In *2011 Proceedings IEEE INFOCOM*. IEEE.
- JANEWAY JR, C. A., TRAVERS, P., WALPORT, M. and SHLOMCHIK, M. J. (2001). The structure of a typical antibody molecule. In *Immunobiology: The Immune System in Health and Disease. 5th edition*. Garland Science.
- JANKOVA, J. and VAN DE GEER, S. (2015). Confidence intervals for high-dimensional inverse covariance estimation. *Electronic Journal of Statistics* **9** 1205–1229.
- JIN, Y., WANG, Z. and LU, J. (2020). Computational and statistical tradeoffs in inferring combinatorial structures of ising model. In *International Conference on Machine Learning*. PMLR.
- JUMPER, J., EVANS, R., PRITZEL, A., GREEN, T., FIGURNOV, M., RONNEBERGER, O., TUNYASUVUNAKOOL, K., BATES, R., ŽÍDEK, A., POTAPENKO, A. ET AL. (2021). Highly accurate protein structure prediction with alphafold. *Nature* **596** 583–589.
- KELMAN, Z. and O'DONNELL, M. (1995). DNA polymerase III holoenzyme: structure and function of a chromosomal replicating machine. *Annual Review of Biochemistry* **64** 171–200.
- KOVACEV-NIKOLIC, V., BUBENIK, P., NIKOLIC, D. and HEO, G. (2016). Using persistent homology and dynamical distances to analyze protein binding. *Statistical Applications in Genetics and Molecular Biology* **15** 19–38.
- LAM, C. and FAN, J. (2009). Sparsistency and rates of convergence in large covariance matrix estimation. *Annals of Statistics* **37** 4254.
- LEE, H., KANG, H., CHUNG, M. K., KIM, B.-N. and LEE, D. S. (2012). Persistent brain network homology from the perspective of dendrogram. *IEEE Transactions on Medical Imaging* **31** 2267–2277.
- LEE, R. K.-W., HOANG, T.-A. and LIM, E.-P. (2019). Discovering hidden topical hubs and authorities across multiple online social networks. *IEEE Transactions on Knowledge and Data Engineering* **33** 70–84.
- LI, J. and MAATHUIS, M. H. (2021). Ggm knockoff filter: False discovery rate control for gaussian graphical models. *Journal of the Royal Statistical Society: Series B (Statistical Methodology)* **83** 534–558.
- LI, Y., FAN, J., WANG, Y. and TAN, K.-L. (2018). Influence maximization on social graphs: A survey. *IEEE Transactions on Knowledge and Data Engineering* **30** 1852–1872.
- LIU, L., WANG, P., NAIR, M. S., YU, J., RAPP, M., WANG, Q., LUO, Y., CHAN, J. F.-W., SAHI, V., FIGUEROA, A. ET AL. (2020). Potent neutralizing antibodies against multiple epitopes on SARS-CoV-2 spike. *Nature* **584** 450–456.
- LIU, W. (2013). Gaussian graphical model estimation with false discovery rate control. *The Annals of Statistics* **41** 2948–2978.
- LIU, Y., FANG, E. X. and LU, J. (2023). Lagrangian inference for ranking problems. *Operations Research* **71** 202–223.
- LU, J., NEYKOV, M. and LIU, H. (2017). Adaptive inferential method for monotone graph invariants. *arXiv preprint arXiv:1707.09114* .
- MEINSHAUSEN, N. and BÜHLMANN, P. (2006). High-dimensional graphs and variable selection with the Lasso. *The Annals of Statistics* **34** 1436–1462.
- MICHALOWICZ, J., NICHOLS, J., BUCHOLTZ, F. and OLSON, C. (2009). An Isserlis’ theorem for mixed Gaussian variables: Application to the auto-bispectral density. *Journal of Statistical Physics* **136** 89–102.
- NEYKOV, M. and LIU, H. (2019). Property testing in high-dimensional Ising models. *The Annals of Statistics* **47** 2472–2503.
- NEYKOV, M., LU, J. and LIU, H. (2019). Combinatorial inference for graphical models. *The Annals of Statistics* **47** 795–827.

- NEYKOV, M., NING, Y., LIU, J. S. and LIU, H. (2018). A unified theory of confidence regions and testing for high-dimensional estimating equations. *Statistical Science* **33** 427–443.
- NIKOLAKAKIS, K. E., KALOGERIAS, D. S. and SARWATE, A. D. (2021). Predictive learning on hidden tree-structured ising models. *Journal of Machine Learning Research* **22** 1–82.
- OU, X., LIU, Y., LEI, X., LI, P., MI, D., REN, L., GUO, L., GUO, R., CHEN, T., HU, J. ET AL. (2020). Characterization of spike glycoprotein of SARS-CoV-2 on virus entry and its immune cross-reactivity with SARS-CoV. *Nature Communications* **11** 1620.
- PENG, J., WANG, P., ZHOU, N. and ZHU, J. (2009). Partial correlation estimation by joint sparse regression models. *Journal of the American Statistical Association* **104** 735–746.
- RAVIKUMAR, P., WAINWRIGHT, M. J. and LAFFERTY, J. D. (2010). High-dimensional ising model selection using ℓ -regularized logistic regression. *The Annals of Statistics* **38** 1287–1319.
- RAVIKUMAR, P., WAINWRIGHT, M. J., RASKUTTI, G. and YU, B. (2011). High-dimensional covariance estimation by minimizing ℓ_1 -penalized log-determinant divergence. *Electronic Journal of Statistics* **5** 935–980.
- RAY, D., LE, L. and ANDRICIOAEI, I. (2021). Distant residues modulate conformational opening in SARS-CoV-2 spike protein. *Proceedings of the National Academy of Sciences* **118** e2100943118.
- REN, Z., SUN, T., ZHANG, C.-H. and ZHOU, H. H. (2015). Asymptotic normality and optimalities in estimation of large Gaussian graphical models. *The Annals of Statistics* **43** 991–1026.
- SHEN, S. and LU, J. (2023). Combinatorial-probabilistic trade-off: P-values of community property test in the stochastic block models. *IEEE Transactions on Information Theory* .
- SHEN, X., PAN, W. and ZHU, Y. (2012). Likelihood-based selection and sharp parameter estimation. *Journal of the American Statistical Association* **107** 223–232.
- VAN DE GEER, S., BÜHLMANN, P., RITOV, Y. and DEZEURE, R. (2014). On asymptotically optimal confidence regions and tests for high-dimensional models. *Annals of Statistics* **42** 1166–1202.
- WANG, L., LIN, F. V., COLE, M. and ZHANG, Z. (2021). Learning clique subgraphs in structural brain network classification with application to crystallized cognition. *Neuroimage* **225** 117493.
- ZHANG, L. and LU, J. (2024). StarTrek: Combinatorial variable selection with false discovery rate control. *The Annals of Statistics* **52** 78–102.

The Wreaths of KHAN: Uniform Graph Feature Selection with False Discovery Rate Control

Abstract

This document contains the supplementary material to the paper “The Wreaths of KHAN: Uniform Graph Feature Selection with False Discovery Rate Control”. It is organized as follows. In Section **A**, we provide detailed preliminaries on persistent homology. Section **B** proves the theoretical results of subgraph selection on FDR and power. Section **C** proves the theoretical results of on the uFDR and power of KHAN algorithm. Section **D** proves auxiliary results in Section 4. Section **E** proves auxiliary results used in Sections **B** - **D**. Section **F** discusses the algorithm to determine homology bases. Finally, Section **G** presents the simulation results for synthetic data

A Preliminaries of Persistent Homology on Graphical Models

Persistent homology is a powerful tool to analyze the subgraph features on graphs. Comprehensive introductions to persistent homology and its foundational algebraic topology can be found in the literature [Horak et al. \(2009\)](#); [Aktas et al. \(2019\)](#). The primary goal of persistent homology is to measure the lifetime (the birth and death) of certain topological properties (e.g., loops, tetrahedron etc.,) along the evolution of the graph. As edges are added to the graph in order, subgraph features may appear or disappear. The sequence of growing (or diminishing) graphs constructed in the process is known as filtration, as illustrated in Figure 1 (a) in the main paper. The lifespan of each homological feature with respect to the filtration levels can be represented as an interval with left and right end points being the birth and the death time, respectively. All intervals yielded by this filtration process can be visualized as the persistent barcodes (See Figure 1 (b) in the main paper), which distinguish long-lasting subgraph features from short-lived ones.

In order to understand homology group, each filtered graph or arbitrary graph $G_0 = (V, E_0)$ can be associated with its clique complex K , which is a collection of all the complete subgraphs of G_0 . By analyzing this filtered complex, we aim to understand its corresponding persistent homology groups across different filtration levels which capture the evolution of the underlying homological features. To that end, for each clique complex K and order k , one needs to introduce the associated chain groups $C_k(E_0)$, the boundary operators $\partial_k : C_k(E_0) \rightarrow C_{k-1}(E_0)$, the cycle groups $Z_k(E_0) = \ker \partial_k$, where

$$\ker \partial_k = \{z \in C_k(E_0) : \partial_k(z) = \emptyset\}.$$

To understand these definitions, $C_k(E_0)$ is a vector space defined on the set of k -dimensional oriented simplices in K . The elements c of the vector space $C_k(E_0)$ are also denoted as k -chains, $c = \sum_i c_i \sigma_i$, with $\{\sigma_i\}_i$ the set of oriented k -simplices in K and $\{c_i \in \mathbb{R}\}_i$ the particular coefficients that specify the vector c . The boundary operators ∂_k are linear maps defined by their actions on

the oriented simplices $\{\sigma_i\}_i$ in K . More precisely, the image of ∂_k acting on an oriented k -simplex $\sigma = [v_0, v_1, \dots, v_k]$ consists of a linear combination of its oriented k facets in $C_{k-1}(E_0)$:

$$\partial_k(\sigma) = \sum_i (-1)^i [v_0, v_1, \dots, v_{i-1}, v_i, \dots, v_k].$$

The definition of the vector subspaces cycle group $Z_k(E_0) = \ker \partial_k$ follows elementarily from the definition of the chain group.

Essentially, for each order k and each graph G_0 , $Z_k(E_0)$ is the set of cycles which are k -chains with empty boundary. As mentioned in Section 2.1, Throughout this paper, the terms ‘‘homology group’’ and ‘‘cycle group’’ will be used interchangeably. We define persistent homology groups as the sequences of groups $Z_k(E(\mu))$ across various filtration levels.

B Proofs of Theorems on the Graph Feature Selection

B.1 Proof of Theorem 4.7

Recall that by definitions

$$\text{FDP} = \frac{\sum_{j \in \mathcal{H}_0} \psi_j(\hat{\alpha})}{\sum_{j \in [J]} \psi_j(\hat{\alpha})} = \frac{\hat{\alpha} J}{\sum_{j \in [J]} \psi_j(\hat{\alpha})} \cdot \frac{\sum_{j \in \mathcal{H}_0} \psi_j(\hat{\alpha})}{J_0 \hat{\alpha}} \cdot \frac{J_0}{J},$$

where $\psi_j(\alpha)$ is the result of the j -th test at level α where $\psi_j(\alpha) = 1$ if we reject H_{0j} and $\psi_j(\alpha) = 0$ otherwise. And $[J] = \{1, 2, \dots, J\}$ is the set of all hypotheses. The subsequent lemma articulates that $\hat{\alpha}$ defined in Algorithm 1 has an equivalent definition.

Lemma B.1 (Equivalence of α). For the $\hat{\alpha} := j_{\max} q / J$ yielded by the BH procedure, equivalently, we have

$$\hat{\alpha} = \sup \left\{ \alpha > 0 : \frac{\alpha J}{\sum_{j \in [J]} \psi_j(\alpha)} \leq q \right\}.$$

Therefore, to prove Theorem 4.7, it suffices to show that

$$\mathbb{P} \left(\frac{\sum_{j \in \mathcal{H}_0} \psi_j(\hat{\alpha})}{J_0 \hat{\alpha}} \leq 1 + \epsilon \right) = 1 - o(1). \quad (\text{B.1})$$

In order to deal with the randomness of $\hat{\alpha}$, we provide a probability bound on $\hat{\alpha}$ first, i.e.,

$$\mathbb{P} \left(\hat{\alpha} \in [q \tilde{J}_1 / J, q] \right) = 1 - o(1), \quad (\text{B.2})$$

where $\tilde{J}_1 = |\tilde{\mathcal{H}}_1|$ and $\tilde{\mathcal{H}}_1$ is defined in (4.3). To prove (B.2), note that by Lemma B.1 the definition of $\hat{\alpha}$ we have

$$\mathbb{P} \left(q \tilde{J}_1 / J \leq \hat{\alpha} \leq q \right) \geq \mathbb{P} \left(\frac{q \tilde{J}_1 / J \cdot J}{\sum_j \psi_j(q \tilde{J}_1 / J)} \leq q \right) = \mathbb{P} \left(\frac{\tilde{J}_1}{\sum_j \psi_j(q \tilde{J}_1 / J)} \leq 1 \right),$$

where the RHS is $1 - o(1)$ by (B.12) in the proof Theorem 4.8 as $\tilde{\mathcal{H}}_1 \subset [J]$.

Now, utilizing (B.2), we can obtain that

$$\begin{aligned}
\mathbb{P}\left(\frac{\sum_{j \in \mathcal{H}_0} \psi_j(\hat{\alpha})}{J_0 \hat{\alpha}} \leq 1 + \epsilon\right) &\geq \mathbb{P}\left(\hat{\alpha} \in [q\tilde{J}_1/J, q], \frac{\sum_{j \in \mathcal{H}_0} \psi_j(\hat{\alpha})}{J_0 \hat{\alpha}} \leq 1 + \epsilon\right) \\
&\geq \mathbb{P}\left(\hat{\alpha} \in [q\tilde{J}_1/J, q], \sup_{q\tilde{J}_1/J \leq \alpha \leq q} \frac{\sum_{j \in \mathcal{H}_0} \psi_j(\alpha)}{J_0 \alpha} \leq 1 + \epsilon\right) \\
&= \mathbb{P}\left(\hat{\alpha} \in [q\tilde{J}_1/J, q]\right) \cdot \mathbb{P}\left(\sup_{q\tilde{J}_1/J \leq \alpha \leq q} \frac{\sum_{j \in \mathcal{H}_0} \psi_j(\alpha)}{J_0 \alpha} \leq 1 + \epsilon\right).
\end{aligned}$$

So to show (B.1), it suffices to show that

$$\mathbb{P}\left(\sup_{q\tilde{J}_1/J \leq \alpha \leq q} \frac{\sum_{j \in \mathcal{H}_0} \psi_j(\alpha)}{J_0 \alpha} \leq 1 + \epsilon\right) = 1 - o(1). \quad (\text{B.3})$$

To make the analysis of uniform control on an interval w.r.t., α tractable, we introduce

$$t_1 = \bar{\Phi}^{-1}(q), t_m = \bar{\Phi}^{-1}(q\tilde{J}_1/J) \quad (\text{B.4})$$

and choose t_i , $i = 2, 3, \dots, m-1$ such that $t_i - t_{i-1} \asymp 1/\sqrt{\log d}$. Here $\bar{\Phi}$ is the cumulative distribution function of standard Gaussian. So we have

$$\frac{\bar{\Phi}(t_i + O(1/\sqrt{\log d}))}{\bar{\Phi}(t_{i-1} + O(1/\sqrt{\log d}))} = 1 + o(1), \quad \text{for all } i = 1, 2, \dots, m-1. \quad (\text{B.5})$$

Also, for any constant C and any $\alpha \in [\bar{\Phi}(t_i), \bar{\Phi}(t_{i-1})]$, we have

$$\frac{\sum_{j \in \mathcal{H}_0} \psi_j(\bar{\Phi}(t_i))}{J_0 \bar{\Phi}(t_i)} \frac{\bar{\Phi}(t_i)}{\bar{\Phi}(t_{i-1})} \leq \frac{\sum_{j \in \mathcal{H}_0} \psi_j(\alpha)}{J_0 \alpha} \leq \frac{\sum_{j \in \mathcal{H}_0} \psi_j(\bar{\Phi}(t_{i-1}))}{J_0 \bar{\Phi}(t_{i-1})} \frac{\bar{\Phi}(t_{i-1})}{\bar{\Phi}(t_i)}.$$

Hence, to prove (B.3), it suffices to show that for a constant C

$$\max_{1 \leq i \leq m} \frac{\sum_{j \in \mathcal{H}_0} \psi_j(\bar{\Phi}(t_i))}{J_0 \bar{\Phi}(t_i)} \leq 1 + o_P(1). \quad (\text{B.6})$$

We discuss two cases (a) and (b) separately: note that for any $j \in [J]$,

$$\begin{aligned}
(a) : \psi_j(\alpha) = 1 &\iff \sqrt{n}|\widehat{W}_e/\widehat{\sigma}_e| > \bar{\Phi}^{-1}(\alpha/2), \text{ for any } e \in E(F_j); \\
(b) : \psi_j(\alpha) = 1 &\iff \sqrt{n}\widehat{W}_e/\widehat{\sigma}_e > \bar{\Phi}^{-1}(\alpha), \text{ for any } e \in E(F_j).
\end{aligned}$$

Introduce $\{\tilde{t}_i\}_{i=1}^m$ and $\{\bar{t}_i\}_{i=1}^m$ as follow,

$$\tilde{t}_i = \begin{cases} \bar{\Phi}^{-1}(\bar{\Phi}(t_i)/2) & \text{if (a);} \\ t_i & \text{if (b);} \end{cases}, \quad \bar{t}_i := \frac{\tilde{t}_i}{1 + C/\log d} - \frac{C}{\sqrt{\log d}}.$$

Now, by direct calculations, for case (a) we have with probability $1 - o(1)$

$$\begin{aligned}
\max_i \frac{\sum_{j \in \mathcal{H}_0} \psi_j(\bar{\Phi}(t_i))}{J_0 \bar{\Phi}(t_i)} &\leq \max_i \frac{\sum_{j \in \mathcal{H}_0} \mathbb{I}\{\sqrt{n}|\widehat{W}_{e_j}/\widehat{\sigma}_{e_j}| > \tilde{t}_i\}}{J_0 2\bar{\Phi}(\tilde{t}_i)} \\
&\leq \max_i \frac{\sum_{j \in \mathcal{H}_0} \mathbb{I}\{\sqrt{n}|\widehat{W}_{e_j}/\sigma_{e_j}|(1 + C/\log d) > \tilde{t}_i\}}{J_0 2\bar{\Phi}(\tilde{t}_i)} \\
&\leq \max_i \frac{\sum_{j \in \mathcal{H}_0} \mathbb{I}\{(\sqrt{n}|W_{e_j}/\sigma_{e_j}| + \frac{C}{\sqrt{\log d}})(1 + C/\log d) > \tilde{t}_i\}}{J_0 2\bar{\Phi}(\tilde{t}_i)} \\
&= \max_i \frac{\sum_{j \in \mathcal{H}_0} \mathbb{I}\{\sqrt{n}|W_{e_j}/\sigma_{e_j}| > \bar{t}_i\}}{J_0 2\bar{\Phi}(\bar{t}_i)} \frac{\bar{\Phi}(\bar{t}_i)}{\bar{\Phi}(\tilde{t}_i)} \\
&\leq \left(\max_i \frac{\sum_{j \in \mathcal{H}_0} \mathbb{I}\{\sqrt{n}W_{e_j}/\sigma_{e_j} > \bar{t}_i\}}{J_0 2\bar{\Phi}(\bar{t}_i)} + \frac{\sum_{j \in \mathcal{H}_0} \mathbb{I}\{\sqrt{n}W_{e_j}/\sigma_{e_j} < -\bar{t}_i\}}{J_0 2\bar{\Phi}(\bar{t}_i)} \right) (1 + o(1))
\end{aligned}$$

where the first inequality follows from $\psi_j(\alpha) = 1$ implies $|\sqrt{n}\widehat{W}_e/\widehat{\sigma}_e| > \bar{\Phi}^{-1}(\alpha/2)$ for case (a), and the second and the third inequalities follow from Assumption 4.1 with $W_e^* = 0$ for any $e \in N_j$, $j \in \mathcal{H}_0$ where $N_j = \{e \in E(F_j) : W_e^* = 0\}$ under case (a); the last inequality is by noting that $|\bar{t}_i - \tilde{t}_i| = O(1/\sqrt{\log d})$ and (B.5).

For case (b) where $W_e^* = 0$ for any $e \in N_j$, $j \in \mathcal{H}_0$, similarly, we have with probability $1 - o(1)$

$$\max_i \frac{\sum_{j \in \mathcal{H}_0} \psi_j(\bar{\Phi}(t_i))}{J_0 \bar{\Phi}(t_i)} \leq \max_i \frac{\sum_{j \in \mathcal{H}_0} \mathbb{I}\{\sqrt{n}\widehat{W}_{e_j}/\widehat{\sigma}_e > \tilde{t}_i\}}{J_0 \bar{\Phi}(\tilde{t}_i)} \leq \max_i \frac{\sum_{j \in \mathcal{H}_0} \mathbb{I}\{\sqrt{n}W_{e_j}/\sigma_{e_j} > \bar{t}_i\}}{J_0 \bar{\Phi}(\bar{t}_i)} (1 + o(1)).$$

Thus, for both (a) and (b), to show (B.6), it suffices to show

$$\max_i \frac{\sum_{j \in \mathcal{H}_0} \mathbb{I}\{\sqrt{n}W_{e_j}/\sigma_{e_j} > \bar{t}_i\}}{J_0 \bar{\Phi}(\bar{t}_i)} \leq 1 + o_P(1), \quad \max_i \frac{\sum_{j \in \mathcal{H}_0} \mathbb{I}\{\sqrt{n}W_{e_j}/\sigma_{e_j} < -\bar{t}_i\}}{J_0 \bar{\Phi}(\bar{t}_i)} \leq 1 + o_P(1).$$

Further, note that $-W_e/\sigma_e = \frac{1}{n} \sum_{i=1}^n [-\xi_i(e)]$ where $-\xi_i(e)$ is mean-zero and has bounded ψ_1 -orlicz norm, thus by symmetry and union bounds, it suffices to show that for some given choice of $\{e_j\}_j$.

$$\mathbb{P}\left(\left|\frac{\sum_{j \in \mathcal{H}_0} \mathbb{I}\{\sqrt{n}W_{e_j}/\sigma_{e_j} > \bar{t}_i\}}{J_0 \bar{\Phi}(\bar{t}_i)} - 1\right| > \epsilon\right) = o(1/\log d), \quad \text{for each } i = 1, 2, \dots, m. \quad (\text{B.7})$$

Fix i . By Markov inequality,

$$\mathbb{P}\left(\left|\frac{\sum_{j \in \mathcal{H}_0} \mathbb{I}\{\sqrt{n}W_{e_j}/\sigma_{e_j} > \bar{t}_i\}}{J_0 \bar{\Phi}(\bar{t}_i)} - 1\right| > \epsilon\right) \leq \frac{\mathbb{E}\left[\sum_{j \in \mathcal{H}_0} (\mathbb{I}\{\sqrt{n}W_{e_j}/\sigma_{e_j} > \bar{t}_i\} - \bar{\Phi}(\bar{t}_i))^2\right]}{J_0^2 \epsilon^2 \bar{\Phi}^2(\bar{t}_i)} = \text{I} + \text{II}, \quad (\text{B.8})$$

where

$$\begin{aligned}
\text{I} &= \frac{\sum_{j_1, j_2 \in \mathcal{H}_0} \mathbb{P}\{\sqrt{n}W_{e_{j_1}}/\sigma_{e_{j_1}} > \bar{t}_i, \sqrt{n}W_{e_{j_2}}/\sigma_{e_{j_2}} > \bar{t}_i\} - \mathbb{P}\{\sqrt{n}W_{e_{j_1}}/\sigma_{e_{j_1}} > \bar{t}_i\} \mathbb{P}\{\sqrt{n}W_{e_{j_2}}/\sigma_{e_{j_2}} > \bar{t}_i\}}{J_0^2 \epsilon^2 \bar{\Phi}^2(\bar{t}_i)}, \\
\text{II} &= \frac{(\sum_{j \in \mathcal{H}_0} \mathbb{P}\{\sqrt{n}W_{e_j}/\sigma_{e_j} > \bar{t}_i\} - \bar{\Phi}(\bar{t}_i))^2}{J_0^2 \epsilon^2 \bar{\Phi}^2(\bar{t}_i)}.
\end{aligned}$$

For some sufficiently large constant $C > 0$, we introduce

$$\begin{aligned}\mathcal{H}_{01} &= \left\{ (j_1, j_2) \in \mathcal{H}_0 \times \mathcal{H}_0 : j_1 \neq j_2, |\text{Cov}(\xi_1(e_{j_1}), \xi_1(e_{j_2}))| \leq C(\log d)^{-2}(\log \log d)^{-1} \right\}, \\ \mathcal{H}_{02} &= \left\{ (j_1, j_2) \in \mathcal{H}_0 \times \mathcal{H}_0 : j_1 \neq j_2, |\text{Cov}(\xi_1(e_{j_1}), \xi_1(e_{j_2}))| > C(\log d)^{-2}(\log \log d)^{-1} \right\}.\end{aligned}$$

We further decompose I as a sum of I_0 , I_1 and I_2 where

$$\begin{aligned}I_0 &= \sum_{j \in \mathcal{H}_0} \frac{\mathbb{P}\{\sqrt{n}W_{e_j}/\sigma_{e_j} > \bar{t}_i\} - \bar{\Phi}(\bar{t}_i)}{J_0^2 \epsilon^2 \bar{\Phi}^2(\bar{t}_i)} \\ I_1 &= \sum_{(j_1, j_2) \in \mathcal{H}_{01}} \frac{\mathbb{P}\{\sqrt{n}W_{e_{j_1}}/\sigma_{e_{j_1}} > \bar{t}_i, \sqrt{n}W_{e_{j_2}}/\sigma_{e_{j_2}} > \bar{t}_i\} - \mathbb{P}\{\sqrt{n}W_{e_{j_1}}/\sigma_{e_{j_1}} > \bar{t}_i\}\mathbb{P}\{\sqrt{n}W_{e_{j_2}}/\sigma_{e_{j_2}} > \bar{t}_i\}}{J_0^2 \epsilon^2 \bar{\Phi}^2(\bar{t}_i)}, \\ I_2 &= \sum_{(j_1, j_2) \in \mathcal{H}_{02}} \frac{\mathbb{P}\{\sqrt{n}W_{e_{j_1}}/\sigma_{e_{j_1}} > \bar{t}_i, \sqrt{n}W_{e_{j_2}}/\sigma_{e_{j_2}} > \bar{t}_i\} - \mathbb{P}\{\sqrt{n}W_{e_{j_1}}/\sigma_{e_{j_1}} > \bar{t}_i\}\mathbb{P}\{\sqrt{n}W_{e_{j_2}}/\sigma_{e_{j_2}} > \bar{t}_i\}}{J_0^2 \epsilon^2 \bar{\Phi}^2(\bar{t}_i)},\end{aligned}$$

To bound I_0 , I_1 , I_2 and II, by our assumptions that $\xi_1(e)$ has bounded ψ_1 -orlicz norm and therefore has bounded moments for bounded orders, and Lemma 6.1 of Liu (2013), we have

$$\begin{aligned}\left| \mathbb{P}(\sqrt{n}W_{e_j}/\sigma_{e_j} > \bar{t}_i) - \bar{\Phi}(\bar{t}_i) \right| &= o\left(\frac{\bar{\Phi}(\bar{t}_i)}{\log d}\right), \quad \text{for any } j \in \mathcal{H}_0; \quad (\text{B.9}) \\ \left| \mathbb{P}(\sqrt{n}W_{e_{j_1}}/\sigma_{e_{j_1}} > \bar{t}_i, \sqrt{n}W_{e_{j_2}}/\sigma_{e_{j_2}} > \bar{t}_i) - \bar{\Phi}(\bar{t}_i)^2 \right| &= o\left(\frac{\bar{\Phi}^2(\bar{t}_i)}{\log d}\right), \quad \text{for any } (j_1, j_2) \in \mathcal{H}_{01}.\end{aligned} \quad (\text{B.10})$$

Now by definitions and direct calculations with triangle's inequality

$$\begin{aligned}|I_0| &\leq \frac{J_0 \bar{\Phi}(\bar{t}_i) (1 - o(\frac{1}{\log d})) (1 - \bar{\Phi}(\bar{t}_i) (1 - o(\frac{1}{\log d})))}{J_0^2 \epsilon^2 \bar{\Phi}^2(\bar{t}_i)} = O\left(\frac{1}{J_0 \bar{\Phi}(\bar{t}_i)}\right), \\ |I_1| &\leq \frac{J_0^2 o(\frac{\bar{\Phi}^2(\bar{t}_i)}{\log d})}{J_0^2 \epsilon^2 \bar{\Phi}^2(\bar{t}_i)} = o\left(\frac{1}{\log d}\right), \\ |I_2| &\leq \frac{\sum_{(j_1, j_2) \in \mathcal{H}_{02}} 2\mathbb{P}(\sqrt{n}W_{e_{j_1}}/\sigma_{e_{j_1}} > \bar{t}_i)}{J_0^2 \epsilon^2 \bar{\Phi}^2(\bar{t}_i)} = O\left(\frac{|\mathcal{H}_{02}|}{J_0^2 \bar{\Phi}(\bar{t}_i)}\right), \\ |\text{II}| &= \frac{(J_0 \bar{\Phi}(\bar{t}_i) o(1/\log d))^2}{J_0^2 \epsilon^2 \bar{\Phi}^2(\bar{t}_i)} = o\left(\frac{1}{\log^2 d}\right).\end{aligned}$$

where the first and fourth inequalities hold by (B.9); the second inequality holds by (B.10); the third inequality holds by (B.9) and

$$\begin{aligned}\mathbb{P}(\sqrt{n}W_{e_{j_1}}/\sigma_{e_{j_1}} > \bar{t}_i, \sqrt{n}W_{e_{j_2}}/\sigma_{e_{j_2}} > \bar{t}_i) &\leq \mathbb{P}(\sqrt{n}W_{e_{j_1}}/\sigma_{e_{j_1}} > \bar{t}_i), \\ \mathbb{P}(\sqrt{n}W_{e_{j_1}}/\sigma_{e_{j_1}} > \bar{t}_i)\mathbb{P}(\sqrt{n}W_{e_{j_2}}/\sigma_{e_{j_2}} > \bar{t}_i) &\leq \mathbb{P}(\sqrt{n}W_{e_{j_1}}/\sigma_{e_{j_1}} > \bar{t}_i).\end{aligned} \quad (\text{B.11})$$

Note that there exist a selection of e_j from N_j , $1 \leq j \leq d$ such that $|\mathcal{H}_{02}| = S$. Recall that $\bar{\Phi}(\bar{t}_i) \geq q\tilde{J}_1/J$ by (B.4), and our assumption on the dependence that $SJ/(J_0^2\tilde{J}_1) = o(1/\log d)$ and sparsity that $J/(J_0\tilde{J}_1) = o(1/\log d)$, we have

$$\max \{|\mathbb{I}_0|, |\mathbb{I}_1|, |\mathbb{I}_2|, |\mathbb{II}|\} = o\left(\frac{1}{\log d}\right).$$

Combining this with (B.8) and (B.7), we finish the proof of the first claim of this theorem.

For the second claim of this theorem which is about the FDR control, note that for any $\epsilon > 0$,

$$\begin{aligned} \text{FDR} = \mathbb{E}[\text{FDP}] &= \int_0^1 \mathbb{P}(\text{FDP} > t) dt \\ &= \int_0^{q\frac{J_0}{J} + \epsilon} \mathbb{P}(\text{FDP} > t) dt + \int_{q\frac{J_0}{J} + \epsilon}^1 \mathbb{P}(\text{FDP} > t) dt \\ &\leq \left(q\frac{J_0}{J} + \epsilon\right) \cdot 1 + \left(1 - q\frac{J_0}{J} - \epsilon\right) \cdot \mathbb{P}\left(\text{FDP} > q\frac{J_0}{J} + \epsilon\right) \\ &= q\frac{J_0}{J} + \epsilon + o\left(\mathbb{P}\left(\text{FDP} > q\frac{J_0}{J} + \epsilon\right)\right). \end{aligned}$$

By the above inequality and the first claim, we have

$$\limsup_{n, d \rightarrow \infty} \text{FDR} \leq q\frac{J_0}{J} + \epsilon \quad \text{for any } \epsilon > 0,$$

which finishes the proof.

B.2 Proof of Theorem 4.8

Note that $\{\psi_j\}$ hinges on random $\hat{\alpha}$, we first separate out the role of $\hat{\alpha}$ by the following

$$\begin{aligned} \mathbb{P}(\psi_j = 1, \text{ for all } j \in \tilde{\mathcal{H}}_1) &\geq \mathbb{P}\left(\psi_j = 1, \text{ for all } j \in \tilde{\mathcal{H}}_1, \hat{\alpha} \in [q\tilde{J}_1/J, q]\right) \\ &\geq \mathbb{P}\left(\psi_j(\alpha) = 1, \text{ for all } j \in \tilde{\mathcal{H}}_1, \hat{\alpha}, \alpha \in [q\tilde{J}_1/J, q]\right) \\ &= \mathbb{P}\left(\psi_j(\alpha) = 1, \text{ for all } j \in \tilde{\mathcal{H}}_1, \alpha \in [q\tilde{J}_1/J, q]\right) \mathbb{P}(\hat{\alpha} \in [q\tilde{J}_1/J, q]). \end{aligned}$$

Therefore, to show the claim, it suffices to show for any $\alpha \in [q\tilde{J}_1/J, q]$

$$\mathbb{P}(\psi_j(\alpha) = 1, \text{ for all } j \in \tilde{\mathcal{H}}_1) = 1 - o(1) \text{ and } \mathbb{P}(\hat{\alpha} \in [q\tilde{J}_1/J, q]) = 1 - o(1).$$

Note that the second equation is proved in (B.2) in the proof of Theorem 4.7.

Therefore, it suffices to show that for any $\alpha \in [q\tilde{J}_1/J, q]$,

$$\mathbb{P}(\psi_j(\alpha) = 1, \text{ for all } j \in \tilde{\mathcal{H}}_1) = 1 - o(1). \tag{B.12}$$

Consider the two scenarios

$$\begin{aligned} (a): p_e &= 2 - 2\Phi(\sqrt{n}|\widehat{W}_e|/\widehat{\sigma}_e) \\ (b): p_e &= 1 - \Phi(\sqrt{n}\widehat{W}_e/\widehat{\sigma}_e) \end{aligned} \tag{B.13}$$

separately. For Scenario (a), by definitions, for all $e \in E(F_j)$, $\sqrt{n}|\widehat{W}_e/\widehat{\sigma}_e| > \bar{\Phi}^{-1}(\alpha/2)$ implies $\psi_j(\alpha) = 1$, so we have

$$\begin{aligned} \mathbb{P}(\psi_j(\alpha) = 1, \text{ for all } j \in \widetilde{\mathcal{H}}_1) &\geq \mathbb{P}\left(\sqrt{n}|\widehat{W}_e/\widehat{\sigma}_e| > \bar{\Phi}^{-1}(\alpha/2), \text{ for all } e \in E(F_j), j \in \widetilde{\mathcal{H}}_1\right) \\ &\geq 1 - \sum_{e \in \cup_{j \in \widetilde{\mathcal{H}}_1} E(F_j)} \mathbb{P}\left(\sqrt{n}|\widehat{W}_e/\widehat{\sigma}_e| \leq \bar{\Phi}^{-1}(\alpha/2)\right). \end{aligned}$$

Therefore, to show (B.12), by $|\cup_j E(F_j)| \leq |\bar{E}| \leq d^2$ and union bounds, it suffices to show that

$$\mathbb{P}\left(\sqrt{n}|\widehat{W}_e/\widehat{\sigma}_e| \leq \bar{\Phi}^{-1}(\alpha/2)\right) = o(1/d^2), \quad \text{for all } e \in \cup_{j \in \widetilde{\mathcal{H}}_1} E(F_j).$$

To see this, denoting $B := \left\{|\widehat{W}_e - W_e - W_e^*|/\sigma_e \leq C/\log d, |\sigma_e/\widehat{\sigma}_e - 1| \leq C\sqrt{(\log d)/n}\right\}$, we have

$$\begin{aligned} \mathbb{P}\left(|\sqrt{n}\widehat{W}_e/\widehat{\sigma}_e| \leq \bar{\Phi}^{-1}(\alpha/2)\right) &\leq \mathbb{P}\left(|\sqrt{n}\widehat{W}_e/\widehat{\sigma}_e| \leq \bar{\Phi}^{-1}(\alpha/2), B\right) + \mathbb{P}(B^c) \\ &\leq \mathbb{P}\left(\sqrt{n}|W_e + W_e^*|/\sigma_e \leq \bar{\Phi}^{-1}(\alpha/2) + C\frac{C}{\sqrt{\log d}}\right) + o(1/d^2) \\ &\leq \bar{\Phi}\left(\sqrt{n}|W_e^*|/\sigma_e - \bar{\Phi}^{-1}(\alpha/2) - \frac{C}{\sqrt{\log d}}\right)(1 + o(1/\log d)) + o(1/d^2) \\ &= o(1/d^2), \end{aligned}$$

where the first inequality holds by $\mathbb{P}(A) = \mathbb{P}(AB) + \mathbb{P}(AB^c) \leq \mathbb{P}(AB) + \mathbb{P}(B^c)$ for any events A, B ; the second inequality holds by event B with $\log d/\log n = O(1)$; the third inequality holds by (B.9) and the symmetry of W ; the last equality holds by $\bar{\Phi}(t) = \exp(-t^2/2)/(\sqrt{2\pi}t)(1 + o(1))$ for $t \gg 1$ and $|\sqrt{n}W_e^*|/\sigma_e > \sqrt{4\log d}$ for any $e \in E(F_j)$, $j \in \widetilde{\mathcal{H}}_1$.

For Scenario (b), by definitions, for all $e \in E(F_j)$, $\sqrt{n}\widehat{W}_e/\widehat{\sigma}_e > \bar{\Phi}^{-1}(\alpha)$ implies $\psi_j(\alpha) = 1$, similarly, we have

$$\begin{aligned} \mathbb{P}(\psi_j = 1, \text{ for all } j \in \widetilde{\mathcal{H}}_1) &\geq \mathbb{P}\left(\sqrt{n}\widehat{W}_e/\widehat{\sigma}_e > \bar{\Phi}^{-1}(\alpha), \text{ for all } e \in E(F_j), j \in \widetilde{\mathcal{H}}_1\right) \\ &\geq 1 - \sum_{e \in \cup_{j \in \widetilde{\mathcal{H}}_1} E(F_j)} \mathbb{P}\left(\sqrt{n}\widehat{W}_e/\widehat{\sigma}_e \leq \bar{\Phi}^{-1}(\alpha)\right), \end{aligned}$$

and we have

$$\mathbb{P}\left(\sqrt{n}\widehat{W}_e \leq \bar{\Phi}^{-1}(\alpha)\right) \leq \bar{\Phi}\left(\sqrt{n}W_e^* - \bar{\Phi}^{-1}(\alpha) - \frac{C}{\sqrt{\log d}}\right)\left(1 + o\left(\frac{1}{\log d}\right)\right) + o(1/d^2) = o(1/d^2),$$

where the equality is by $\bar{\Phi}(t) \sim \exp(-t^2/2)/(\sqrt{2\pi}t)$ for $t \gg 1$ and $\sqrt{n}W_e^*/\sigma_e > \sqrt{4\log d}$ for any $e \in E(F_j)$, $j \in \widetilde{\mathcal{H}}_1$. This finishes the whole proof.

C Proof of Theorem 4.13

For simplicity of notations, without loss of generality, we assume $\sigma_e = 1$, thereby simplifying $W_e/\sigma_e = W_e$. The core argument of Theorem 4.13 hinges on the following lemma:

Lemma C.1 (Equivalence of Algorithms). The persistent barcodes determined by Algorithm 3 is equivalent to that determined by running Algorithm 2 through the whole filtration line $\mu \geq 0$ in the sense that at each filtration level μ , $\tilde{Z}(\mu)$ are the same.

Based on Lemma C.1, it suffices to develop statistical controls on uFDP and uFDR for the homology group by Algorithm 2 on $\mu \in (\mu_0, \mu_1)$.

To prove Theorem 4.13, we first introduce several notations. Based on the definition of critical edges $\{\bar{e}_j : j = 1, 2, \dots, \bar{J}\}$ in Section 4.2 that \bar{e}_j corresponds to an increase of rank in the homology group. So we define Z_j as the corresponding basis in the homology group. Note that essentially we are considering the following multiple testing problem

$$\bar{H}_{0j}(\mu) : \bar{e}_j \notin E^*(\mu), \quad \text{v.s.} \quad \bar{H}_{1j}(\mu) : \bar{e}_j \in E^*(\mu), \quad j \in [\bar{J}]. \quad (\text{C.1})$$

Let $\bar{\mathcal{H}}_0(\mu) = \{j \in [\bar{J}] : \bar{H}_{0j}(\mu) \text{ is true}\}$ is the set of all true null hypotheses at filtration level μ and $\bar{J}_0(\mu) = |\bar{\mathcal{H}}_0(\mu)|$. We also formally define test results $\psi_{j,\mu}(\alpha)$ at level α , where $\psi_{j,\mu}(\alpha) = 1$ if and only if $Z_j \subseteq \tilde{Z}(\mu)$, and $\psi_{j,\mu}(\alpha) = 0$ otherwise. For brevity, we adopt $\psi_{j,\mu}$ in the subsequent proof, when no ambiguity arises.

Then (2.3) is equivalent to define uFDP and FDP(μ) in the following traditional way:

$$\text{uFDP} = \sup_{\mu \in [\mu_0, \mu_1]} \text{FDP}(\mu), \quad \text{where } \text{FDP}(\mu) = \frac{\sum_{j \in \bar{\mathcal{H}}_0(\mu)} \psi_{j,\mu}(\hat{\alpha}(\mu))}{\max\{1, \sum_{j=1}^{\bar{J}} \psi_{j,\mu}(\hat{\alpha}(\mu))\}}.$$

We also have $\tilde{\mathcal{H}}_1(\mu) = \{j : \bar{H}_{1j}(\mu) \text{ is true with } W_{\bar{e}_j}^*(\mu) > C\sqrt{\log d/n}\}$ and $\tilde{J}_1(\mu) = |\tilde{\mathcal{H}}_1(\mu)|$.

However, due to the absence of prior knowledge regarding the underlying graph structure G^* (which would allow us to directly identify the homology groups), it becomes challenging to ascertain which edges are critical and to distinguish between homological features in each Z_{j-1} . This complexity hampers our ability to devise a definitive decision rule for each hypothesis. Given a selected homological feature, the inherent complexity of the problem limits our capacity to associate it with its respective hypothesis pair, rendering the empirical values of $\{\psi_{j,\mu}\}_j$ unobservable. Despite these obstacles, theoretically, it is still possible to assess $\{\psi_{j,\mu}\}_j$ based on the selected homological features and Z_{j-1} , enabling us to examine the theoretical behavior of uFDP and uFDR.

We first have the following theorem on uFDP control.

Theorem C.2 (General guarantee on tail probability of FDP(μ) for persistent barcodes). Under the same conditions of Theorem 4.13, we have the persistent barcode yielded by Algorithm 2 on a fixed filtration level $\mu \geq 0$ satisfies

$$\sup_{\mu \in [\mu_0, \mu_1]} \text{FDP}(\mu) \leq \frac{q\bar{J}_0(\mu_1)}{\bar{J}} + o_P(1).$$

Then uFDR control follows by Theorem C.2. Note that for any $\epsilon > 0$, we have

$$\begin{aligned} \text{uFDR} &= \mathbb{E}\left[\sup_{\mu \in [\mu_0, \mu_1]} \text{FDP}(\mu)\right] = \int_0^1 \mathbb{P}\left(\sup_{\mu \in [\mu_0, \mu_1]} \text{FDP}(\mu) > t\right) dt \\ &= \int_0^{q\bar{J}_0(\mu_1)/\bar{J} + \epsilon} \mathbb{P}\left(\sup_{\mu \in [\mu_0, \mu_1]} \text{FDP}(\mu) > t\right) dt + \int_{q\bar{J}_0(\mu_1)/\bar{J} + \epsilon}^1 \mathbb{P}\left(\sup_{\mu \in [\mu_0, \mu_1]} \text{FDP}(\mu) > t\right) dt \\ &\leq (q\bar{J}_0(\mu_1)/\bar{J} + \epsilon) \cdot 1 + (1 - \epsilon) \cdot \mathbb{P}\left(\sup_{\mu \in [\mu_0, \mu_1]} \text{FDP}(\mu) > q\bar{J}_0(\mu_1)/\bar{J} + \epsilon\right) \\ &= q\bar{J}_0(\mu_1)/\bar{J} + \epsilon + o(1), \end{aligned}$$

which gives

$$\text{uFDR} \leq \frac{q\bar{J}_0(\mu_1)}{\bar{J}} + o(1) + \epsilon, \quad \text{for any } \epsilon > 0.$$

Secondly for power analysis, we have the following theorem.

Theorem C.3 (General guarantee on power for persistent barcodes). Under the same conditions of Theorem 4.13, we have the persistent barcode yielded by Algorithm 2 on a fixed filtration level $\mu \geq 0$ satisfies

$$\mathbb{P}\left(Z(\mu + C\sqrt{\log d/n}) \subseteq \widehat{Z}(\mu) \text{ for all } \mu \in [\mu_0, \mu_1]\right) = 1 - o(1).$$

C.1 Proof of Theorem C.2

The structure of this proof is similar to the proof of Theorem 4.7. For simplicity, we only highlight the key steps.

With $\widehat{\alpha}$ defined in Algorithm 2, we employ this notation $\widehat{\alpha}(\mu)$ specifically when executing Algorithm 2 at the filtration level μ . Note that

$$\text{FDP}(\mu) - \frac{q\bar{J}_0(\mu_1)}{\bar{J}} = \frac{\sum_{j \in \bar{\mathcal{H}}_0(\mu)} \psi_{j,\mu}(\widehat{\alpha}(\mu))}{\sum_{j \in [\bar{J}]} \psi_{j,\mu}(\widehat{\alpha}(\mu))} - \frac{q\bar{J}_0(\mu_1)}{\bar{J}} = \left(\frac{\widehat{\alpha}(\mu)\bar{J}}{\sum_{j \in [\bar{J}]} \psi_{j,\mu}(\widehat{\alpha}(\mu))} \cdot \frac{\sum_{j \in \bar{\mathcal{H}}_0(\mu)} \psi_{j,\mu}(\widehat{\alpha}(\mu))}{\bar{J}_0(\mu_1)\widehat{\alpha}(\mu)} - q \right) \cdot \frac{\bar{J}_0(\mu_1)}{\bar{J}},$$

where $\bar{J}_0(\mu) = |\bar{\mathcal{H}}_0(\mu)|$. By Lemma B.1, the BHq procedure is equivalent to have

$$\widehat{\alpha}(\mu) = \sup \left\{ \alpha : \frac{\alpha\bar{J}}{\sum_{j \in [\bar{J}]} \psi_{j,\mu}(\alpha)} \leq q \right\},$$

where $\psi_{j,\mu}(\alpha)$ is the test result at level α . Therefore, to prove FDP control, it suffices to show that

$$\mathbb{P}\left(\sup_{\mu \in [\mu_0, \mu_1]} \frac{\sum_{j \in \bar{\mathcal{H}}_0(\mu)} \psi_{j,\mu}(\widehat{\alpha}(\mu))}{\bar{J}_0(\mu_1)\widehat{\alpha}(\mu)} \leq 1 + \epsilon \right) = 1 - o(1), \quad \forall \epsilon > 0. \quad (\text{C.2})$$

Similarly, to deal with the randomness of $\widehat{\alpha}(\mu)$, we follow the proofs of Theorem 4.7 and Theorem C.3. We have

$$\mathbb{P}\left(\widehat{\alpha}(\mu) \in \left[\frac{q\widetilde{J}_1(\mu)}{\bar{J}}, q\right], \text{ for all } \mu \in [\mu_0, \mu_1]\right) = 1 - o(1), \quad (\text{C.3})$$

where recall that $\tilde{\mathcal{H}}_1(\mu) = |\tilde{\mathcal{H}}_1(\mu)|$. Therefore, we have

$$\begin{aligned}
& \mathbb{P}\left(\sup_{\mu \in [\mu_0, \mu_1]} \frac{\sum_{j \in \tilde{\mathcal{H}}_0(\mu)} \psi_{j,\mu}(\hat{\alpha}(\mu))}{\bar{J}_0(\mu_1) \hat{\alpha}(\mu)} \leq 1 + \epsilon\right) \\
& \geq \mathbb{P}\left(\frac{\sum_{j \in \tilde{\mathcal{H}}_0(\mu)} \psi_{j,\mu}(\hat{\alpha}(\mu))}{\bar{J}_0(\mu_1) \hat{\alpha}(\mu)} \leq 1 + \epsilon, \hat{\alpha}(\mu) \in \left[\frac{q \tilde{J}_1(\mu)}{\bar{J}}, q\right], \text{ for all } \mu \in [\mu_0, \mu_1]\right) \\
& \geq \mathbb{P}\left(\sup_{\substack{\alpha \in [q \tilde{J}_1(\mu_1)/\bar{J}, q] \\ \mu \in [\mu_0, \mu_1]}} \frac{\sum_{j \in \tilde{\mathcal{H}}_0(\mu)} \psi_{j,\mu}(\alpha)}{\bar{J}_0(\mu_1) \alpha} \leq 1 + \epsilon, \sup_{\mu \in [\mu_0, \mu_1]} \hat{\alpha}(\mu) \in \left[\frac{q \tilde{J}_1(\mu)}{\bar{J}}, q\right]\right) \\
& \geq \mathbb{P}\left(\sup_{\substack{\alpha \in [q \tilde{J}_1(\mu_1)/\bar{J}, q] \\ \mu \in [\mu_0, \mu_1]}} \frac{\sum_{j \in \tilde{\mathcal{H}}_0(\mu)} \psi_{j,\mu}(\alpha)}{\bar{J}_0(\mu_1) \alpha} \leq 1 + \epsilon\right) - \mathbb{P}\left(\sup_{\mu \in [\mu_0, \mu_1]} \hat{\alpha}(\mu) \in \left[\frac{q \tilde{J}_1(\mu)}{\bar{J}}, q\right]\right) \\
& \geq \mathbb{P}\left(\sup_{\substack{\alpha \in [q \tilde{J}_1(\mu_1)/\bar{J}, q] \\ \mu \in [\mu_0, \mu_1]}} \frac{\sum_{j \in \tilde{\mathcal{H}}_0(\mu)} \psi_{j,\mu}(\alpha)}{\bar{J}_0(\mu_1) \alpha} \leq 1 + \epsilon\right) - o(1)
\end{aligned}$$

where the first inequality is by narrowing down the event; the second inequality is because $\hat{\alpha}(\mu) \in [q \tilde{J}_1(\mu)/\bar{J}, q]$ implies $\hat{\alpha}(\mu) \subset [q \tilde{J}_1(\mu_1)/\bar{J}, q]$ for all $\mu \in [\mu_0, \mu_1]$; the last inequality is by (C.3).

Now we see that in order to show (C.2), it suffices to show that for any $\mu \in [\mu_0, \mu_1]$ we have

$$\sup_{\mu \in [\mu_0, \mu_1]} \sup_{q \tilde{J}_1(\mu_1)/\bar{J} \leq \alpha \leq q} \frac{\sum_{j \in \tilde{\mathcal{H}}_0(\mu)} \psi_{j,\mu}(\alpha)}{\bar{J}_0(\mu_1) \alpha} \leq 1 + o_P(1), \quad (\text{C.4})$$

where we note that the two supremums can be exchanged.

We discuss two cases (a) and (b) separately: note that for any $j \in [\bar{J}]$,

$$\begin{aligned}
(a) : \psi_{j,\mu}(\alpha) = 1 & \implies \sqrt{n}(|\widehat{W}_{\bar{e}_j}| - \mu)/\widehat{\sigma}_{\bar{e}_j} > \bar{\Phi}^{-1}(\alpha/2), \text{ (e.g., Gaussian graphical models)} \\
(b) : \psi_{j,\mu}(\alpha) = 1 & \implies \sqrt{n}(\widehat{W}_{\bar{e}_j} - \mu)/\widehat{\sigma}_{\bar{e}_j} > \bar{\Phi}^{-1}(\alpha), \text{ (e.g., Ising models)}.
\end{aligned} \quad (\text{C.5})$$

Consider case (b) first, where $W_{\bar{e}_j}^* \leq \mu$ for $j \in \tilde{\mathcal{H}}_0(\mu)$. Directly, for each $j \in \tilde{\mathcal{H}}_0(\mu)$

$$\psi_{j,\mu}(\alpha) \leq \mathbb{I}\{\sqrt{n}(\widehat{W}_{\bar{e}_j} - \mu)/\widehat{\sigma}_{\bar{e}_j} > \bar{\Phi}^{-1}(\alpha)\} \leq \mathbb{I}\{\sqrt{n}(\widehat{W}_{\bar{e}_j} - W_{\bar{e}_j}^*)/\widehat{\sigma}_{\bar{e}_j} > \bar{\Phi}^{-1}(\alpha)\}.$$

Combining this with $\tilde{\mathcal{H}}_0(\mu) \subset \tilde{\mathcal{H}}_0(\mu_1)$, it follows that

$$\sup_{\mu \in [\mu_0, \mu_1]} \sum_{j \in \tilde{\mathcal{H}}_0(\mu)} \psi_{j,\mu}(\alpha) \leq \sum_{j \in \tilde{\mathcal{H}}_0(\mu_1)} \mathbb{I}\{\sqrt{n}(\widehat{W}_{\bar{e}_j} - W_{\bar{e}_j}^*)/\widehat{\sigma}_{\bar{e}_j} > \bar{\Phi}^{-1}(\alpha)\}.$$

And so to show (C.4), it suffices to show

$$\sup_{q \tilde{J}_1(\mu_1)/\bar{J} \leq \alpha \leq q} \frac{\sum_{j \in \tilde{\mathcal{H}}_0(\mu_1)} \mathbb{I}\{\sqrt{n}(\widehat{W}_{\bar{e}_j} - W_{\bar{e}_j}^*)/\widehat{\sigma}_{\bar{e}_j} > \bar{\Phi}^{-1}(\alpha)\}}{\bar{J}_0(\mu_1) \alpha} \leq 1 + o_P(1)$$

Then, with $\{t_i\}_i$ introduced in (B.5), by similar argument in the proof of Theorem 4.7, for (b), it suffices to show

$$\text{for (b): } \max_{1 \leq i \leq m} \frac{\sum_{j \in \tilde{\mathcal{H}}_0(\mu_1)} \mathbb{I}\{\sqrt{n}(\widehat{W}_{\bar{e}_j} - W_{\bar{e}_j}^*)/\widehat{\sigma}_{\bar{e}_j} > t_i\}}{\bar{J}_0(\mu_1) \bar{\Phi}(t_i)} \leq 1 + o_P(1), \quad (\text{C.6})$$

and similarly

$$\text{for (a): } \max_{1 \leq i \leq m} \frac{\sum_{j \in \bar{\mathcal{H}}_0(\mu_1)} \mathbb{I}\{\sqrt{n}(|\widehat{W}_{\bar{e}_j}| - |W_{\bar{e}_j}^*|)/\widehat{\sigma}_{\bar{e}_j} > \bar{\Phi}^{-1}(\bar{\Phi}(t_i)/2)\}}{\bar{J}_0(\mu_1)\bar{\Phi}(t_i)} \leq 1 + o_P(1). \quad (\text{C.7})$$

To study the effect of the estimators, we introduce $\{\tilde{t}_i\}_{i=1}^m$ and $\{\bar{t}_i\}_{i=1}^m$ as follows:

$$\tilde{t}_i = \begin{cases} \bar{\Phi}^{-1}(\bar{\Phi}(t_i)/2) & \text{if (a);} \\ t_i & \text{if (b);} \end{cases}, \quad \bar{t}_i = \frac{\tilde{t}_i}{1 + C\sqrt{(\log d)/n}} - \frac{C}{\sqrt{\log d}}.$$

Similar to the analysis in Section B.1. For case (b) where $W_{\bar{e}_j}^* \leq \mu$ for $j \in \bar{\mathcal{H}}_0(\mu)$, we have with probability $1 - o(1)$

$$\begin{aligned} \max_{1 \leq i \leq m} \frac{\sum_{j \in \bar{\mathcal{H}}_0(\mu_1)} \mathbb{I}\{\sqrt{n}(\widehat{W}_{\bar{e}_j} - W_{\bar{e}_j}^*)/\widehat{\sigma}_{\bar{e}_j} > t_i\}}{\bar{J}_0(\mu_1)\bar{\Phi}(t_i)} &= \max_i \frac{\sum_{j \in \bar{\mathcal{H}}_0(\mu)} \mathbb{I}\{\sqrt{n}(\widehat{W}_{\bar{e}_j} - W_{\bar{e}_j}^*)/\widehat{\sigma}_{\bar{e}_j} > \tilde{t}_i\}}{\bar{J}_0(\mu_1)\bar{\Phi}(\tilde{t}_i)} \\ &\leq \max_i \frac{\sum_{j \in \bar{\mathcal{H}}_0(\mu)} \mathbb{I}\{W_{\bar{e}_j} > \tilde{t}_i\}}{\bar{J}_0(\mu_1)\bar{\Phi}(\tilde{t}_i)} \\ &\leq \max_i \frac{\sum_{j \in \bar{\mathcal{H}}_0(\mu)} \mathbb{I}\{W_{\bar{e}_j} > \tilde{t}_i\} \bar{\Phi}(\tilde{t}_i)}{\bar{J}_0(\mu_1)\bar{\Phi}(\tilde{t}_i) \bar{\Phi}(\tilde{t}_i)}, \end{aligned}$$

where second to last inequality holds by assumption on \widehat{W} and $\widehat{\sigma}$ and the assumption that $\sigma_e = 1$.

On the other hand, for the case (a) with that $|W_{\bar{e}_j}^*| \leq \mu$, $j \in \bar{\mathcal{H}}_0(\mu)$, similarly, we have with probability $1 - o(1)$

$$\begin{aligned} \max_{1 \leq i \leq m} \frac{\sum_{j \in \bar{\mathcal{H}}_0(\mu_1)} \mathbb{I}\{\sqrt{n}(|\widehat{W}_{\bar{e}_j}| - |W_{\bar{e}_j}^*|)/\widehat{\sigma}_{\bar{e}_j} > t_i\}}{\bar{J}_0(\mu_1)\bar{\Phi}(t_i)} \\ \leq \max_i \left(\frac{\sum_{j \in \bar{\mathcal{H}}_0(\mu_1)} \mathbb{I}\{W_{\bar{e}_j} > \bar{t}_i\}}{\bar{J}_0(\mu_1)2\bar{\Phi}(\bar{t}_i)} + \frac{\sum_{j \in \bar{\mathcal{H}}_0(\mu_1)} \mathbb{I}\{W_{\bar{e}_j} < -\bar{t}_i\}}{\bar{J}_0(\mu_1)2\bar{\Phi}(\bar{t}_i)} \right) \frac{\bar{\Phi}(\bar{t}_i)}{\bar{\Phi}(\bar{t}_i)}. \end{aligned}$$

By $\frac{\bar{\Phi}(\bar{t}_i)}{\bar{\Phi}(\bar{t}_i)} = 1 + o(1)$ obtained in Section B.1, it can be seen that for either case (a) or (b), to show (C.6), it suffices to show

$$\max_i \frac{\sum_{j \in \bar{\mathcal{H}}_0(\mu_1)} \mathbb{I}\{W_{\bar{e}_j} > \bar{t}_i\}}{\bar{J}_0(\mu_1)\bar{\Phi}(\bar{t}_i)} \leq 1 + o_P(1), \quad \max_i \frac{\sum_{j \in \bar{\mathcal{H}}_0(\mu_1)} \mathbb{I}\{W_{\bar{e}_j} < -\bar{t}_i\}}{\bar{J}_0(\mu_1)\bar{\Phi}(\bar{t}_i)} \leq 1 + o_P(1).$$

The procedure to prove the probability bounds on the RHS of the above inequalities is the same as that in the rest proof of Theorem 4.7 and so we omit the details.

C.2 Proof of Theorem C.3

The proof is similar to the proof of Theorem 4.8 but they are conceptually different. Similarly, by the definition of $\psi_{j,\mu}(\alpha)$, it suffices to show that for any $\alpha \in [q\tilde{J}_1(\mu)/\bar{J}, q]$,

$$\mathbb{P}(\psi_{j,\mu}(\alpha) = 1, \text{ for all } j \in \bar{\mathcal{H}}_1(\mu), \mu \in [\mu_0, \mu_1]) = 1 - o(1).$$

We consider Scenario (b) in (C.5) first. We have

$$\begin{aligned}
& \mathbb{P}(\psi_{j,\mu}(\alpha) = 1, \text{ for all } j \in \tilde{\mathcal{H}}_1(\mu), \mu \in [\mu_0, \mu_1]) \\
& \geq \mathbb{P}\left(\sqrt{n}\widehat{W}_e(\mu)/\widehat{\sigma}_e > \bar{\Phi}^{-1}(\alpha), \text{ for all } e \text{ with } W_e^* \geq \mu + \sqrt{\frac{4 \log d}{n}}, \mu \in [\mu_0, \mu_1]\right) \\
& \geq \mathbb{P}\left(W_e + W_e^* - \frac{C}{\sqrt{n \log d}} - \mu > \frac{\bar{\Phi}^{-1}(\alpha)}{\sqrt{n}}, \text{ for all } e \text{ with } W_e^* \geq \mu + \sqrt{\frac{4 \log d}{n}}, \mu \in [\mu_0, \mu_1]\right) \\
& \geq \mathbb{P}\left(W_e + \sqrt{\frac{4 \log d}{n}} - \frac{C}{\sqrt{n \log d}} > \frac{\bar{\Phi}^{-1}(\alpha)}{\sqrt{n}}, \text{ for all } e \in E\right) \\
& \geq 1 - \sum_{e \in E} \mathbb{P}\left(W_e + \sqrt{\frac{4 \log d}{n}} - \frac{C}{\sqrt{n \log d}} < \frac{\bar{\Phi}^{-1}(\alpha)}{\sqrt{n}}\right),
\end{aligned}$$

where the second inequality is because \widehat{W}_e satisfies $\mathbb{P}(\sup_{e \in E} |\widehat{W}_e - W_e - W_e^*| > \frac{C}{\sqrt{n \log d}}) < o(1)$ since we assume $\sigma_e = 1$; the third inequality is by direct bounds; the last inequality is by union bound.

For Scenario (a) in (C.5), similarly, we have

$$\begin{aligned}
& \mathbb{P}(\psi_{j,\mu}(\alpha) = 1, \text{ for all } j \in \tilde{H}_1(\mu), \mu \in [\mu_0, \mu_1]) \\
& \geq \mathbb{P}\left(\sqrt{n}|\widehat{W}_e(\mu)|/\widehat{\sigma}_e > \bar{\Phi}^{-1}(\alpha/2), \text{ for all } e \text{ with } |W_e^*| \geq \mu + \sqrt{\frac{4 \log d}{n}}, \mu \in [\mu_0, \mu_1]\right) \\
& \geq \mathbb{P}\left(|W_e^*| - |W_e| - \mu - \frac{C}{\sqrt{n \log d}} > \frac{\bar{\Phi}^{-1}(\alpha/2)}{\sqrt{n}} \text{ for all } e \text{ with } |W_e^*| \geq \mu + \sqrt{\frac{4 \log d}{n}}, \mu \in [\mu_0, \mu_1]\right) \\
& \geq 1 - \sum_{e \in E} \mathbb{P}\left(|W_e| + \sqrt{\frac{4 \log d}{n}} - \frac{C}{\sqrt{\log d}} < \frac{\bar{\Phi}^{-1}(\alpha/2)}{\sqrt{n}}, \text{ for all } e \in E\right),
\end{aligned}$$

where the second inequality is by $\mathbb{P}(\sup_{e \in E} |\widehat{W}_e - W_e - W_e^*| > \frac{C}{\sqrt{n \log d}}) < o(1)$; the third is by union bound.

At the same time, by (B.9) and elementary calculations with $\bar{\Phi}(t) \sim \exp(-t^2/2)/(\sqrt{2\pi}t)$ for $t \gg 1$

$$\mathbb{P}\left(W_e + \sqrt{\frac{4 \log d}{n}} - \frac{C}{\sqrt{\log d}} < \bar{\Phi}^{-1}(\alpha)\right) = o(1/d^2), \quad \text{for any } e \in E.$$

It is seen that, for both Scenarios (a) and (b) with any $\alpha \in [q\tilde{J}_1(\mu)/\bar{J}, q]$

$$\mathbb{P}(\psi_{j,\mu}(\alpha) = 1, \text{ for all } j \in \tilde{H}_1(\mu), \mu \in [\mu_0, \mu_1]) \geq 1 - \sum_{e \in E} o(1/d^2) = 1 - o(1). \quad (\text{C.8})$$

This finishes the proof.

D Proofs of Propositions 4.2-4.3 and Corollaries 4.14-4.15

D.1 Proof of Proposition 4.2

By Lemma L.4 in [Neykov et al. \(2019\)](#) and that for GGM $\sigma_{uv} = \sqrt{\Theta_{uu}^* \Theta_{vv}^*}$ with $\|\Theta^*\|_1 \leq M$, we directly obtain

$$\mathbb{P}\left(\sup_{e \in \bar{E}} |\widehat{W}_e - W_e - W_e^*|/\sigma_e \leq \frac{C}{\sqrt{n \log d}}\right) = 1 - o(1).$$

At the same time, adjusting the coefficient of $\log d$ in (D.36) in [Zhang and Lu \(2024\)](#) can show that

$$\sup_{e \in \bar{E}} |\widehat{\Theta}_e^d - \Theta_e^*| = O_P\left(\sqrt{\frac{\log d}{n}}\right),$$

which implies that

$$\mathbb{P}\left(\sup_{e \in \bar{E}} |\sigma_e/\widehat{\sigma}_e - 1| \leq C\sqrt{\frac{\log d}{n}}\right) = 1 - o(1).$$

Combining the above with union bound, we obtain the result of this proposition.

Last, by $\|X - \mathbb{E}[X]\|_{\psi_1} \leq C\|X\|_{\psi_1}$ and $\|XY\|_{\psi_1} \leq \|X\|_{\psi_2}\|Y\|_{\psi_2}$, we have for any $(u, v) \in \bar{E}$,

$$\|\xi_1((u, v))\|_{\psi_1} \leq C \left\| \frac{\Theta_u^* X X^\top \Theta_v^*}{\sqrt{\Theta_{uu}^* \Theta_{vv}^*}} \right\|_{\psi_1} \leq C \left\| \frac{\Theta_u^* X}{\sqrt{\Theta_{uu}^*}} \right\|_{\psi_2} \left\| \frac{\Theta_v^* X}{\sqrt{\Theta_{vv}^*}} \right\|_{\psi_2} = C.$$

This finishes the whole proof.

D.2 Proof of Proposition 4.3

By definitions, for Ising model, we directly have

$$\widehat{W}_e - W_e - W_e^* = 0.$$

It is left to prove the claim on $\widehat{\sigma}_e$.

For simplicity of notations, we introduce, for any $(u, v) \in V \times V$,

$$\widehat{m}_{uv} = \frac{1}{n} \sum_{i=1}^n X_{iu} X_{iv}, \quad m_{uv} = \mathbb{E}[X_u X_v].$$

By definitions, for any $e \in \bar{E}$, we can write,

$$\frac{\sigma_e}{\widehat{\sigma}_e} - 1 = \frac{(\widehat{m}_e - m_e)(\widehat{m}_e + m_e)}{\sqrt{1 - \widehat{m}_e^2}(\sqrt{1 - \widehat{m}_e^2} + \sqrt{1 - m_e^2})}.$$

To bound the RHS, we first bound $|\widehat{m}_e - m_e|$, which relies on the following lemma:

Lemma D.1 (Auxillary results for Ising models). For Ising model with $W^* \in \mathcal{W}$ defined in (2.10), and $\log d/\log n = O(1)$, we have for some positive constants C ,

$$1 - \sup_{e \in \bar{E}} m_e^2 \geq C \log^3 d/n.$$

This lemma allows us to utilize Bernstein inequality:

$$|\widehat{m}_e - m_e| = O_P\left(\sqrt{\frac{\log d}{n}(1 - m_e^2)}\right).$$

Further, combining this with $|m_e|, |\widehat{m}_e| \leq 1$, we have

$$|1 - \widehat{m}_e^2 - (1 - m_e^2)| = |\widehat{m}_e - m_e| \cdot |\widehat{m}_e + m_e| = O_P\left(\sqrt{\frac{\log d}{n}(1 - m_e^2)}\right) = o_P(1 - m_e^2),$$

where the equality is because $1 - m_e^2 \geq C \log^3 d/n$.

It is seen that $1 - \widehat{m}_e^2 = (1 - m_e^2)(1 + o(1)) \geq C \log^3 d/n$. And it follows that

$$\left|\frac{\sigma_e}{\widehat{\sigma}_e} - 1\right| = O_P\left(\frac{\log d}{n} \frac{1}{\sqrt{\log^3 d/n}}\right) = O_P\left(\frac{1}{\log d}\right),$$

which finishes the proof of the claim on $\widehat{\sigma}$.

Last, for each $(u, v) \in \bar{E}$, to see $\xi_1((u, v)) = \frac{X_u X_v - \mathbb{E}[X_u X_v]}{\sqrt{\text{Var}(X_u X_v)}}$ has bounded ψ_1 -orlicz norm. Note that

$$\text{Var}(X_u X_v) = 4(1 - m_{uv}^2) \geq C \text{ and } |X_u X_v - \mathbb{E}[X_u X_v]| \leq 2,$$

it can be seen that $\xi_1((u, v))$ is a bounded random variable and so has bounded ψ_1 -orlicz norm. This finishes all the proofs of the lemma.

D.3 Proof of Proposition 4.5

For any valid dependent set $\mathcal{S} \in \mathbb{S}$ and any $(j_1, j_2) \in \mathcal{S}$, there exist $(u, v) \in N_{j_1}$ and $(u', v') \in N_{j_2}$ such that $|\text{Cov}(\xi_1(u, v), \xi_1(u', v'))| \geq C(\log d)^{-2}(\log \log d)^{-1}$, and for the Gaussian graphical model, we have

$$|\text{Cov}(\xi_1(u, v), \xi_1(u', v'))| = \frac{|\Theta_{uu'}^* \Theta_{vv'}^* + \Theta_{uv'}^* \Theta_{u'v}^*|}{\sqrt{\Theta_{uu}^* \Theta_{u'u}^* \Theta_{vv}^* \Theta_{v'v'}^*}}.$$

Thus, we can bound S by

$$\begin{aligned} S &= \left| \left\{ (j_1, j_2) : j_1, j_2 \in \mathcal{H}_0, j_1 \neq j_2, \exists (u, v) \in N_{j_1}, (u', v') \in N_{j_2} \text{ s.t. } |\text{Cov}(\xi_1(u, v), \xi_1(u', v'))| \geq \frac{C(\log d)^{-2}}{\log \log d} \right\} \right| \\ &= \sum_{j_1 \in \mathcal{H}_0} \sum_{j_2 \in \mathcal{H}_0} \mathbb{I} \left\{ \exists (u, v) \in N_{j_1}, (u', v') \in N_{j_2} \text{ s.t. } |\text{Cov}(\xi_1(u, v), \xi_1(u', v'))| \geq C(\log d)^{-2}(\log \log d)^{-1} \right\} \\ &\leq |\mathcal{H}_0| \max_{j_1 \in \mathcal{H}_0, (u, v) \in N_{j_1}} \sum_{j_2 \in \mathcal{H}_0} \mathbb{I} \left\{ \exists (u', v') \in N_{j_2} \text{ s.t. } |\text{Cov}(\xi_1(u, v), \xi_1(u', v'))| \geq C(\log d)^{-2}(\log \log d)^{-1} \right\} \\ &\leq |\mathcal{H}_0| \max_{j_1 \in \mathcal{H}_0, (u, v) \in N_{j_1}} \sum_{j_2 \in \mathcal{H}_0} \sum_{(u', v') \in N_{j_2}} \mathbb{I} \left\{ |\text{Cov}(\xi_1(u, v), \xi_1(u', v'))| \geq C(\log d)^{-2}(\log \log d)^{-1} \right\} \\ &= |\mathcal{H}_0| \max_{j_1 \in \mathcal{H}_0, (u, v) \in N_{j_1}} \sum_{(u', v') \in \bar{E}} \sum_{j_2 \in \mathcal{H}_0: (u', v') \in N_{j_2}} \mathbb{I} \left\{ |\text{Cov}(\xi_1(u, v), \xi_1(u', v'))| \geq C(\log d)^{-2}(\log \log d)^{-1} \right\} \\ &= |\mathcal{H}_0| \max_{j_1 \in \mathcal{H}_0, (u, v) \in N_{j_1}} \sum_{(u', v') \in \bar{E}} \mathbb{I} \left\{ |\text{Cov}(\xi_1(u, v), \xi_1(u', v'))| \geq C(\log d)^{-2}(\log \log d)^{-1} \right\} \sum_{j_2 \in \mathcal{H}_0: (u', v') \in N_{j_2}} 1. \end{aligned} \tag{D.1}$$

So in the following proof, we assume j_1 and (u, v) are fixed. Then, the edge (u', v') satisfying

$$|\text{Cov}(\xi_1(u, v), \xi_1(u', v'))| = \frac{|\Theta_{uu'}^* \Theta_{vv'}^* + \Theta_{uv'}^* \Theta_{u'v}^*|}{\sqrt{\Theta_{uu}^* \Theta_{u'u}^* \Theta_{vv}^* \Theta_{v'v'}^*}} \geq C(\log d)^{-2}(\log \log d)^{-1}$$

must satisfy $\Theta_{uu'}^* \Theta_{vv'}^* + \Theta_{uv'}^* \Theta_{u'v}^* \neq 0$, which results in one of the two following cases for u' and v' :

$$\text{Case 1: } (u, u') \in E^* \text{ and } (v, v') \in E^*; \quad \text{Case 2: } (u, v') \in E^* \text{ and } (v, u') \in E^*.$$

Since we fixed (u, v) and the maximum degree of G^* is s , we have s choices of u' and s choices of v' for any fixed (u, v) .

Then we fix (u', v') , and aim to bound $\sum_{j_2 \in \mathcal{H}_0: (u', v') \in N_{j_2}} 1$, which is the number of $j_2 \in \mathcal{H}_0$ satisfying $(u', v') \in N_{j_2}$. We have

$$\sum_{j_2 \in \mathcal{H}_0} \mathbb{I}\{(u', v') \in N_{j_2}\} \leq \sum_{j_2 \in \mathcal{H}_0} \mathbb{I}\{(u', v') \in E(F_{j_2})\} \leq \binom{d}{M-2},$$

where the first inequality holds by (4.4) the $N_j \subseteq E(F_j)$. Thus we finally have $S = O(s^2 d^{M-2} |\mathcal{H}_0|)$.

D.4 Proof of Proposition 4.6

For Ising models, we have

$$|\text{Cov}(\xi_1(u, v), \xi_1(u', v'))| = \text{Cov}(X_u X_v, X_{u'} X_{v'}).$$

In Lemma 15 of Nikolakakis et al. (2021), it is proved that for any tree structure $G = (V, E)$ and any even-sized set of nodes $V' \subseteq V$, V' can be partitioned into $|V'|/2$ pairs of nodes, such that the paths connecting each pair are disjoint with each other. So four nodes u, u', v, v' can be divided into two pairs and gives two disjoint paths. We denote $\mathcal{CP}_G(u, u', v, v')$ as the collection of edges in the two edge-disjoint paths (so we have $\mathcal{CP}_G(u, u', v, v') \subseteq E$). Then by Theorem 10 in Nikolakakis et al. (2021), if u, v, u', v' are on the same tree, we immediately have

$$\mathbb{E}(X_u X_v X_{u'} X_{v'}) = \prod_{(i,j) \in \mathcal{CP}_G(u, u', v, v')} \mathbb{E}(X_i X_j) = \prod_{(i,j) \in \mathcal{CP}_G(u, u', v, v')} \tanh(w_{ij}^*),$$

where the last equality follows from Lemma 14 in Nikolakakis et al. (2021).

Further, for forest structure $G = \cup_\ell T_\ell$ where T_ℓ is the ℓ -th tree of the forest G , we have

$$\mathbb{E}(X_u X_v X_{u'} X_{v'}) = \prod_{(i,j) \in \cup_\ell \mathcal{CP}_{T_\ell}(u, u', v, v')} \mathbb{E}(X_i X_j) = \prod_{(i,j) \in \cup_\ell \mathcal{CP}_{T_\ell}(u, u', v, v')} \tanh(w_{ij}^*)$$

from Section 4.4 in Nikolakakis et al. (2021). In addition, in forest-structu graph models, for any node i and j , Lemmas 13 and 14 in Nikolakakis et al. (2021) give

$$\mathbb{E}(X_i X_j) = \prod_{e \in \text{path}(i,j)} \tanh(w_e^*).$$

Thus, we have

$$\begin{aligned} \text{Cov}(X_u X_v, X_{u'} X_{v'}) &= \mathbb{E}(X_u X_v X_{u'} X_{v'}) - \mathbb{E}(X_u X_v) \mathbb{E}(X_{u'} X_{v'}) \\ &= \prod_{(i,j) \in \cup_\ell \mathcal{CP}_{T_\ell}(u, u', v, v')} \tanh(w_{ij}^*) - \prod_{e \in \text{path}(u,v)} \tanh(w_e^*) \prod_{e \in \text{path}(u', v')} \tanh(w_e^*). \end{aligned} \quad (\text{D.2})$$

Now, we are ready to give a bound for S . Similar to (D.1), S can be bounded by

$$\begin{aligned}
S &\leq |\mathcal{H}_0| \max_{j_1 \in \mathcal{H}_0, (u,v) \in N_{j_1}} \sum_{(u',v') \in \bar{E}} \mathbb{I}\left\{ |\text{Cov}(\xi_1(u,v), \xi_1(u',v'))| \geq C(\log d)^{-2}(\log \log d)^{-1} \right\} \sum_{j_2 \in \mathcal{H}_0: (u',v') \in N_{j_2}} 1 \\
&\leq |\mathcal{H}_0| \max_{j_1 \in \mathcal{H}_0, (u,v) \in N_{j_1}} \sum_{(u',v') \in \bar{E}} \mathbb{I}\left\{ |\text{Cov}(\xi_1(u,v), \xi_1(u',v'))| \neq 0 \right\} \sum_{j_2 \in \mathcal{H}_0: (u',v') \in N_{j_2}} 1 \\
&= |\mathcal{H}_0| \max_{j_1 \in \mathcal{H}_0, (u,v) \in N_{j_1}} \sum_{(u',v') \in \bar{E}} \mathbb{I}\left\{ \mathbb{E}(X_u X_v X_{u'} X_{v'}) - \mathbb{E}(X_u X_v) \mathbb{E}(X_{u'} X_{v'}) \neq 0 \right\} \sum_{j_2 \in \mathcal{H}_0} \mathbb{I}\{(u',v') \in N_{j_2}\}.
\end{aligned}$$

By (D.2), for fixed (u,v) , the edge (u',v') satisfying $\mathbb{E}(X_u X_v X_{u'} X_{v'}) - \mathbb{E}(X_u X_v) \mathbb{E}(X_{u'} X_{v'}) \neq 0$ must satisfy one of the two following cases:

(i) u, u', v, v' are in two different trees with two nodes in each tree, and u, v must be in the same tree, and u', v' must be in the other tree. So we have $O(\frac{d}{s})$ potential choices of the second tree for u', v' , and $O(s^2)$ choices of u', v' .

(ii) u, u', v, v' are in the same tree, and $\text{path}(u,v) \cap \text{path}(u',v') \neq \emptyset$. We have $\cup_{\ell} \mathcal{CP}_{T_\ell}(u, u', v, v') = \text{path}(u, u') \cup \text{path}(v, v')$ and thus $\mathbb{E}(X_u X_v X_{u'} X_{v'}) - \mathbb{E}(X_u X_v) \mathbb{E}(X_{u'} X_{v'}) \neq 0$. So we have $O(s^2)$ choices of u', v' .

At the same time, when fixing (u',v') , we have

$$\sum_{j_2 \in \mathcal{H}_0} \mathbb{I}\{(u',v') \in N_{j_2}\} \leq \sum_{j_2 \in \mathcal{H}_0} \mathbb{I}\{(u',v') \in E(F_{j_2})\} \leq \binom{d}{M-2}.$$

Thus we finally have

$$S = O\left(|\mathcal{H}_0| \left(\frac{d}{s} s^2 + s^2\right) \binom{d}{M-2}\right) = O(|\mathcal{H}_0| d^{M-1} s).$$

D.5 Proof of Proposition 4.12

For the Gaussian graphical model, similar to the proof in Section D.3, we have under persistent homology

$$\begin{aligned}
\bar{S}(\mu) &= \left| \left\{ (j_1, j_2) : j_1 \neq j_2, \bar{e}_{j_1}, \bar{e}_{j_2} \notin E^*(\mu), |\text{Cov}(\xi_1(\bar{e}_{j_1}), \xi_1(\bar{e}_{j_2}))| \geq \frac{C}{(\log d)^2 \log(\log d)} \right\} \right| \\
&\leq \left| \left\{ (j_1, j_2) : j_1 \neq j_2, (u,v) = \bar{e}_{j_1} \notin E^*, (u',v') = \bar{e}_{j_2} \notin E^*, |\text{Cov}(\xi_1(u,v), \xi_1(u',v'))| \neq 0 \right\} \right| \\
&\leq \sum_{j_1} \mathbb{I}\{(u,v) = \bar{e}_{j_1} \notin E^*\} \max_{j_1, (u,v)} \sum_{(u',v') = \bar{e}_{j_2} \notin E^*} \mathbb{I}\left\{ |\text{Cov}(\xi_1(u,v), \xi_1(u',v'))| \neq 0 \right\} \sum_{j_2: (u',v') = \bar{e}_{j_2} \notin E^*} 1 \\
&\leq \sum_{j_1} \mathbb{I}\{(u,v) = \bar{e}_{j_1} \notin E^*\} \max_{j_1, (u,v)} \sum_{(u',v') = \bar{e}_{j_2} \notin E^*} \mathbb{I}\left\{ \Theta_{uu'}^* \Theta_{vv'}^* + \Theta_{uv'}^* \Theta_{u'v}^* \neq 0 \right\} \sum_{j_2: (u',v') = \bar{e}_{j_2} \notin E^*} 1.
\end{aligned}$$

First we have $\sum_{j_1} \mathbb{I}\{(u,v) = \bar{e}_{j_1} \notin E^*\} = |\bar{\mathcal{H}}_0(\mu)|$ because only if $j_1 \in \bar{\mathcal{H}}_0(\mu)$ then $\bar{e}_{j_1} \notin E^*$.

Then we assume j_1 and (u,v) are fixed. Similar to the proof in Section D.3, to satisfy $\Theta_{uu'}^* \Theta_{vv'}^* + \Theta_{uv'}^* \Theta_{u'v}^* \neq 0$, we have $O(s(\mu)^2)$ choices of critical edge (u',v') , where $s(\mu)$ is the maximum degree of $G^*(\mu)$.

Next we fix (u',v') , and aim to bound $\sum_{j_2: (u',v') = \bar{e}_{j_2} \notin E^*} 1$, which is the number of j_2 having critical edge $\bar{e}_{j_2} = (u',v')$. Recall that we defined $R = \max_{i=1}^{|\bar{E}|} \ell_i$ Section 4.2, so one critical edge can increase at most R rank, i.e., correspond to at most R hypotheses. So $\sum_{j_2: (u',v') = \bar{e}_{j_2} \notin E^*} 1 = O(R)$.

Thus, for the Gaussian graphical model, we finally have

$$\bar{S}(\mu) = O(|\bar{\mathcal{H}}_0(\mu)| \cdot s(\mu)^2 R).$$

For the Ising model, similar to the argument in Section D.4, we have

$$\bar{S}(\mu) = O(|\bar{\mathcal{H}}_0(\mu)| \cdot s(\mu) dR).$$

D.6 Proof of Corollary 4.9

By Proposition 4.2 for GGM, the three claims of this corollary follows from Theorem 4.7-4.8 if we set for any $j \in \mathcal{H}_0$ and $e = (u, v) \in \bar{E}$

$$N_j = \{e \in E(F_j) : \Theta_e^* = 0\}, \quad W_{uv} = \sum_{i=1}^n \Theta_u^{*\top} (X_i X_i^\top \Theta_v^* - e_v) / n, \quad W_e^* = \Theta_e^*.$$

It remains to check the sparsity and dependence conditions are matched. To see this, by Isserlis' theorem (Theorem 1.1 in Michalowicz et al. (2009)), and so

$$\text{Cov}(\Theta_u^{*\top} (X X^\top \Theta_v^* - e_v) / \sqrt{\Theta_{uu}^* \Theta_{vv}^*}, \Theta_{u'}^{*\top} (X X^\top \Theta_{v'}^* - e_{v'}) / \sqrt{\Theta_{u'u'}^* \Theta_{v'v'}^*}) = \frac{W_{uu'}^* W_{vv'}^* + W_{uv'}^* W_{u'v}^*}{\sqrt{W_{uu}^* W_{vv}^*}}.$$

This finishes the proof.

D.7 Proof of Corollary 4.10

Recall m and \hat{m} are introduced in Section D.2. By Proposition 4.3 for Ising model, the three claims of this corollary follows from Theorems 4.7-4.8 if we set

$$N_j = \{e \in E(F_j) : W_e^* \leq 0\}, \quad W_{uv} = \frac{1}{n} \sum_{i=1}^n X_{iu} X_{iv} - m_{uv}$$

and

$$W_{uv}^* = m_{uv} - \tanh(\theta)$$

for any $j \in \mathcal{H}_0$, $(u, v) \in \bar{E}$. The covariance calculations for Ising model are straightforward and so we omit it. This finishes the proof.

D.8 Proofs of Corollaries 4.14-4.15

The proofs of Corollaries 4.14-4.15 follow by Propositions 4.2-4.3 and Theorem 4.13. The procedures are the same as that of Corollaries 4.9-4.10. We omit the details.

E Proofs of Auxiliary Lemmas

E.1 Auxiliary Proposition for Persistent Homology

The following proposition gives a explicit formula for the dimension of the homology group of a complete graph.

Proposition E.1. The dimension of the k -homology group of a d -clique is $(d - k)(d - k - 1)/2$.

By the above property, it can be seen that the dimension of each k -homology group is $O(d^2)$. In the ordinary subgraph selection, the number of testing triangles in a graph requires $\binom{d}{3}$ hypotheses. This suggests that persistent homology is a more reasonable way to select hole-structure graph features as it rules out redundancy.

Proof. For a k -th homology group of a d -clique, its dimension is equivalent to all ways to add the edges to the graph along the filtration. Denote $A_d^k = \dim(Z_k(E_{d \times d}))$. We are going to develop a recurrence relation between A_i^k and A_{i-1}^k . Note that for a $(i - 1)$ -clique, if we add a extra node and connect the node with the original $i - 1$ nodes. The process is equivalent to the filtration process to complementing a $(i - 1)$ -clique with an isolated node to a i -clique. Noting that for k -th homology group, the first extra k -clique appears after the $k - 1$ edges connecting the isolated node and the original $i - 1$ nodes. After that each new edge induces a new k -th clique. There are $i - 1$ less edges for a $(i - 1)$ -clique compared to a i -clique. Therefore, $Z_k(E_{i \times i})$ has extra $(i - 1) - (k + 1 - 1)$ dimension than $Z_k(E_{(i-1) \times (i-1)})$:

$$A_i^k = A_{i-1}^k + i - k - 1.$$

Solving this recursive relation with $A_k^k = 1$, we get

$$A_d^k = (d - k)(d - k - 1)/2,$$

which finishes this proof. □

E.2 Proof of Lemma B.1

The core of proving equivalence is to show

$$\sup \left\{ \alpha > 0 : \frac{\alpha J}{\sum_{j \in [J]} \psi_j(\alpha)} \leq q \right\} \geq \frac{q j_{\max}}{J} \text{ and } \sup \left\{ \alpha > 0 : \frac{\alpha J}{\sum_{j \in [J]} \psi_j(\alpha)} \geq q \right\} \geq \frac{q j_{\max}}{J}. \quad (\text{E.1})$$

First, noting that $j_{\max} = \sum_{j \in [J]} \psi_j(\frac{q j_{\max}}{J})$, we have

$$\frac{\alpha J}{\sum_{j \in [J]} \psi_j(\alpha)} \Big|_{\alpha = q j_{\max}/J} = q,$$

which implies that

$$\sup \left\{ \alpha > 0 : \frac{\alpha J}{\sum_{j \in [J]} \psi_j(\alpha)} \leq q \right\} \geq \frac{q j_{\max}}{J}.$$

Next, we prove the second part of (E.1) by contradiction. Let us presume

$$\tilde{\alpha} = \sup \left\{ \alpha > 0 : \frac{\alpha J}{\sum_{j \in [J]} \psi_j(\alpha)} \leq q \right\} > \frac{q j_{\max}}{J}. \quad (\text{E.2})$$

By definitions,

$$\tilde{\alpha} < p_{(j_{\max} + 1)}, \text{ the } (j_{\max} + 1)\text{-th smallest } p\text{-value};$$

otherwise $\frac{\alpha J}{\sum_{j \in [J]} \psi_j(\alpha)} \Big|_{\alpha=p_{j_{(\max+1)}}} \leq q$ suggests that rejected hypotheses are at least $j_{\max} + 1$ and lead to contradiction. By monotonicity of $\psi_j(\alpha)$ and definitions of $\tilde{\alpha}$,

$$\tilde{\alpha} \leq \frac{q \sum_{j \in [J]} \psi_j(\tilde{\alpha})}{J} < \frac{q \sum_{j \in [J]} \psi_j(p_{(j_{\max+1})})}{J} = \frac{q(j_{\max} + 1)}{J}.$$

It remains to demonstrate the impossibility of $\frac{q(j_{\max})}{J} < \tilde{\alpha} < \frac{q(j_{\max+1})}{J}$. By (E.2), we have

$$\frac{\alpha J}{\sum_{j \in [J]} \psi_j(\alpha)} \Big|_{\alpha=\tilde{\alpha}} > \frac{\frac{q(j_{\max})}{J} J}{\sum_{j \in [J]} \psi_j(\tilde{\alpha})} = \frac{\frac{q(j_{\max})}{J} J}{\sum_{j \in [J]} \psi_j(\frac{q(j_{\max})}{J})} = q,$$

which contradicts the definition of $\tilde{\alpha}$ and finishes the proof.

E.3 Proof of Lemma C.1

We aim to show that Algorithm 3 and Algorithm 2 give the same homology group $\widehat{Z}(\mu)$ for any filtration level μ . By definition, the edge sets constructing the homology group are identical for the two algorithms at $\mu = 0$ and $\mu > \mu^{(t)}$. Recall that in Algorithm 3, we obtain the homology group $\widehat{Z}^{(t+1)} = \widehat{Z}(\mu^{(t+1)})$. Therefore, it remains to prove the following claims:

(i) In Algorithm 2, the set of selected homology group is right-continuous i.e., $\widehat{Z}(\mu)$ stays the same for $\mu \in [\mu^{(s)}, \mu^{(s+1)})$, for each $s = 0, 1, \dots, t-1$;

To prove (i), recall that according to Algorithm 3, at iteration s , $\widehat{Z}^{(s)}$ is the homology group from the previous iteration. By the definitions of $\mu^{(s+1)} = \min_{e \in E^{(s)}} \text{lower bound of weight}_e(\text{rank}(\widehat{Z}^{(s)})q/\bar{J})$. Therefore, by the nature of BHq procedure, the selected homology group between $[\mu^{(s)}, \mu^{(s+1)})$ stays the same and we finishes the proof.

E.4 Proof of Lemma D.1

Consider the claim on m_e first. By similar idea of the proof of Lemma C.3 in Neykov and Liu (2019), we can show that for any $e \in \bar{E}$

$$|m_e| \leq \tanh(w_e^*) + \sum_{m \geq 2} s(s-1)^{m-2} \tanh^m(\Theta) \leq \tanh(w_e^*) + \frac{\text{stanh}^2(\Theta)}{1 - (s-1)\tanh(\Theta)}. \quad (\text{E.3})$$

By the conditions $\|w^*\|_\infty \leq \Theta$, $\text{stanh}(\Theta) < \rho$ and $s \geq 2\rho/(1-\rho)$, we have

$$\tanh(w_e^*) + \frac{\text{stanh}^2(\Theta)}{1 - (s-1)\tanh(\Theta)} \leq \tanh(\Theta) + \tanh(\Theta) \frac{\rho}{1-\rho} \leq \frac{\rho}{s(1-\rho)} \leq \frac{1}{2}.$$

It follows that $1 - m_e^2 \geq 3/4 \gg C \log^3 d/n$. This finishes the proof.

F Algorithm for Determining the Importance Scores

When searching for homology, edges are added sequentially and loops are searched for according to two principles. The first principle is to find the loop that contains the most nodes from the distance data. If multiple loops have the same number of nodes from the distance features, then search for the loop with the largest average edge weight. Record the loops found in this way.

Algorithm 4: Homology Search Algorithm

```
1 Input: Trajectory Data  $X_\phi$  and  $X_\psi$ , Distance Data  $X_d$ , FDR level  $q$ , Filtration Level  $\mu$ .
2 Build a d-dimensional Gaussian graphical model based on  $X_\phi$ ,  $X_\psi$  and  $X_d$ .
3 for  $\mu_i \in \mu$  do
4   Get Edge Set  $E^{(i)} = \widehat{E}(\mu_i)$  applying DGS;
5   Get estimated edge weights  $\{\widehat{W}_e\}_{e \in E^{(i)}}$ 
6   for  $e \in E^{(i)}$  do
7     Find all the loops linking the two nodes of  $e$ ;
8     Select the loop that has the most nodes from  $X_d$ ;
9     if Any two loops have the same number of nodes from the distance data then
10      | Select the loop with the largest average edge weight according to  $\{\widehat{W}_e\}_{e \in E^{(i)}}$ 
11      end
12   end
13 end
14 Output: Homologies Set  $H(\mu)$ 
```

G Numerical Experiments for Synthetic Data

In this section, we examine the performance our method through numerical simulations. We first consider the general subgraph selection. For the Gaussian graphical model and the Ising model in Sections 2.3 and 2.4, in particular, we focus on the performance of the proposed method as we vary the dimension d , sample size $n \in \{300, 350, 400\}$, the nominal level $q \in \{0.05, 0.1\}$ and the types of sub-graphs. For illustration, in the Gaussian graphical model, we focus on the detection of triangles, four-cycles and five-cycles, while in the Ising model, we focus on the detection of five-trees, which are trees consisting of five nodes with three possible shapes, as illustrated in Figure 7. We estimate the empirical FDR and power based on 100 repetitions.

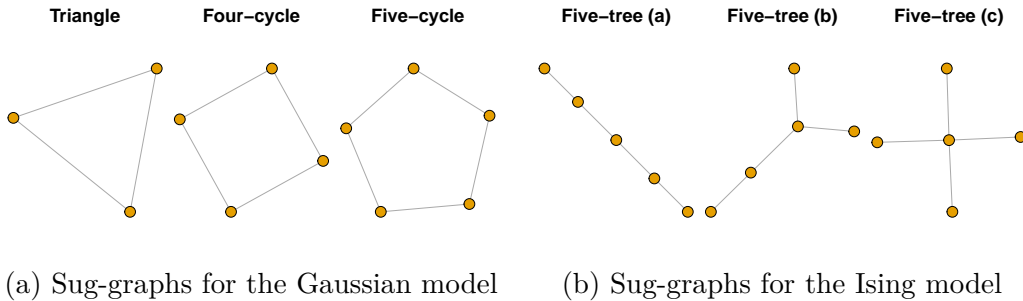


Figure 7: Sub-graphs to test for the Gaussian graphical model and the Ising model.

The Gaussian graphical model is generated as follows. First, we generate the adjacency matrix consisting of triangles, four-cycles and five-cycles: $3m_1$ nodes form m_1 triangles, $4m_2$ nodes form m_2 four-cycles, and $5m_3$ nodes form m_3 five-cycles, while these sub-graphs have no overlapping nodes with each other. Then dimension $d = 3m_1 + 4m_2 + 5m_3$. To make the problem more challenging, we randomly add one edge to the four-cycles and three edges to the five-cycles with an example of the adjacency matrix illustrated in Figure 8 (a). We then generate the entries of precision matrix Θ^* by sampling from Uniform(0.85, 1) for edges in the adjacency graph and setting

other entries as zero. Finally, we add a small value $v = 0.1$ together with the absolute value of the minimal eigenvalue of Θ^* to the diagonal elements of Θ^* to ensure its positive-definiteness. We take different combinations of (m_1, m_2, m_3) : $(20, 10, 20)$, $(20, 10, 30)$, $(40, 20, 20)$ and $(60, 30, 10)$, which yield $d = 200, 250, 300$ and 350 , respectively.

The Ising model is generated similarly where the adjacency graph consisting of m -trees with m sampled uniformly from 6 to 10 as illustrated by Figure 8 (b). The dimension d is also chosen from $\{200, 250, 300, 350\}$ where the last few nodes (with size smaller than m) are set to be disconnected with all other nodes. We sample w_e^* from $\text{Uniform}(0.9, 1)$ for all edges e 's in the adjacency graph and set $w_e^* = 0$ otherwise. The thresholding value θ in (2.12) is set as 0.45.



(a) Graph of the Gaussian graphical model (b) Graph of the Ising model

Figure 8: Examples of the adjacency graphs used for the Gaussian graphical model and the Ising model.

The results for the Gaussian graphical model is presented in Table 1. We can see that the FDRs of all configurations are well controlled by their nominal level q while the power is pretty good for all configurations. Specifically, with the sample size n increases, the FDRs tend to decrease. The FDRs for detection triangles are larger than those of four-cycles and five-cycles since there are more hypotheses to test for four cycles and five cycles compared to triangles.

The results for the Ising model is presented in Table 2. The similar pattern is observed as the Gaussian graphical model. All FDRs are below the nominal level q for different values of n, d and q . The power increases quickly as the sample size n increases. The results of the five-tree (a) and five-tree (b) are more similar compared to that of five-tree (c), as the numbers of hypotheses are same for testing five-tree (a) and five-tree (b).

We then consider the testing for persistent homology. Since the true correlation graph in Ising model does not have a explicit form, we only consider the Gaussian graphical model for the simulation in this part.

The model is generated in a similar way to the above setting. First, we generate the adjacency matrix consisting of triangles, four-cliques, and five-cliques: $3m_1$ nodes form m_1 triangles, $4m_2$ nodes form m_2 four-cliques, and $5m_3$ nodes form m_3 five-cliques, while these sub-graphs have no overlapping nodes with each other. We then randomly reduce the edges of five cliques with probability $p = 0.1$. An example of the adjacency matrix is illustrated in Figure 9. The sample size n is 400 and the dimension d is $3m_1 + 4m_2 + 5m_3$. We then generate the entries of the precision matrix Θ^* by sampling from $\text{Uniform}(0, 10)$ for edges in the adjacency graph and setting other entries as zero. Finally, we add a small value $v = 0.25$ together with the absolute value of the minimal eigenvalue of Θ^* to the diagonal elements of Θ^* to ensure its positive definiteness. We set (m_1, m_2, m_3) : $(10, 30, 10)$, which yields $d = 200$ respectively. The filtration level is set between 0 and 1.

Table 1: Empirical FDR and power averaged over 100 repetitions in the detection of triangles, four-cycles and five-cycles under the Gaussian graphical model.

q	0.05			0.1			0.05			0.1		
n	300	350	400	300	350	400	300	350	400	300	350	400
	FDR						Power					
d	(i) Triangle											
200	0.031	0.025	0.020	0.040	0.033	0.025	0.999	1.000	1.000	0.999	1.000	1.000
250	0.036	0.034	0.033	0.046	0.045	0.042	0.999	1.000	1.000	1.000	1.000	1.000
300	0.029	0.030	0.030	0.037	0.037	0.039	0.999	1.000	1.000	1.000	1.000	1.000
400	0.029	0.025	0.026	0.036	0.031	0.032	1.000	1.000	1.000	1.000	1.000	1.000
d	(ii) Four-cycle											
200	0.011	0.008	0.005	0.014	0.011	0.007	0.996	1.000	1.000	0.997	1.000	1.000
250	0.012	0.013	0.012	0.016	0.016	0.016	0.992	0.999	1.000	0.994	1.000	1.000
300	0.011	0.009	0.009	0.013	0.012	0.012	0.992	0.998	1.000	0.994	0.999	1.000
400	0.011	0.010	0.011	0.014	0.013	0.014	0.990	0.998	1.000	0.992	0.999	1.000
d	(iii) Five-cycle											
200	0.001	0.002	0.001	0.001	0.002	0.001	0.961	0.988	0.997	0.964	0.989	0.997
250	0.003	0.004	0.003	0.004	0.005	0.003	0.958	0.987	0.994	0.965	0.988	0.994
300	0.002	0.003	0.002	0.003	0.003	0.002	0.941	0.981	0.992	0.947	0.982	0.993
400	0.001	0.002	0.002	0.002	0.002	0.003	0.914	0.976	0.993	0.925	0.979	0.994

Table 2: Empirical FDR and power averaged over 100 repetitions in the detection of triangles, four-cycles and five-cycles under the Ising model.

q	0.05			0.1			0.05			0.1		
n	300	350	400	300	350	400	300	350	400	300	350	400
	FDP						Power					
d	Five-tree (a)											
200	0.014	0.020	0.032	0.018	0.024	0.040	0.531	0.770	0.888	0.575	0.800	0.902
250	0.011	0.013	0.025	0.013	0.018	0.030	0.461	0.744	0.870	0.505	0.774	0.886
300	0.009	0.012	0.016	0.011	0.014	0.020	0.452	0.678	0.838	0.492	0.710	0.857
400	0.005	0.007	0.012	0.006	0.009	0.014	0.379	0.627	0.834	0.416	0.661	0.851
d	Five-tree (b)											
200	0.017	0.024	0.037	0.021	0.030	0.046	0.524	0.775	0.889	0.571	0.802	0.903
250	0.012	0.017	0.027	0.014	0.022	0.032	0.479	0.748	0.881	0.515	0.777	0.899
300	0.010	0.011	0.021	0.012	0.013	0.026	0.464	0.687	0.841	0.505	0.719	0.861
400	0.006	0.009	0.012	0.007	0.011	0.017	0.398	0.631	0.837	0.431	0.671	0.857
d	Five-tree (c)											
200	0.016	0.030	0.026	0.017	0.033	0.032	0.420	0.579	0.732	0.450	0.606	0.754
250	0.013	0.022	0.026	0.015	0.025	0.032	0.402	0.611	0.764	0.437	0.640	0.778
300	0.008	0.011	0.019	0.010	0.011	0.028	0.384	0.568	0.729	0.428	0.593	0.747
400	0.007	0.008	0.010	0.008	0.011	0.018	0.358	0.524	0.747	0.385	0.551	0.776

The results for the Gaussian graphical model are presented in Figure 10. We can see that the FDR is well controlled by their nominal level q while the power is above 0.4. Specifically, as the filter level increases, the FDR tends to decrease.

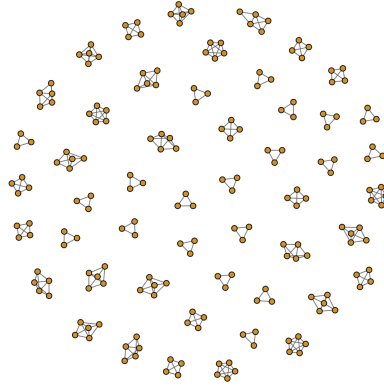


Figure 9: Graph of the Gaussian graphical model for persistent homology

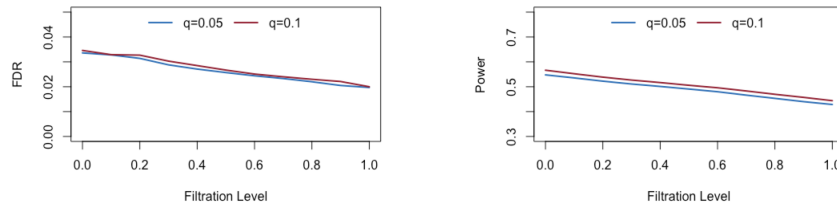


Figure 10: Empirical FDR and power averaged over 100 repetitions in the detection of homology under the Gaussian graphical model.